Title: Structure of long-range direct and indirect spinocerebellar pathways as well as local spinal circuits mediating proprioception.

Abbreviated Title: Long-range and local proprioceptive circuits.

Author names and affiliations:

Iliodora V. Pop[1], Felipe Espinosa[1], Cheasequah J. Blevins[5,6], Portia C. Okafor[1], Osita W. Ogujiofor[1], Megan Goyal[1], Bishakha Mona[1], Mark A. Landy[1], Kevin M. Dean[2], Channabasavaiah B. Gurumurthy[3, 4], Helen C. Lai[1]

[1] Dept. of Neuroscience, UT Southwestern Medical Center, Dallas, TX 75390

[2] Dept. of Cell Biology, UT Southwestern Medical Center, Dallas, TX 75390

[3] Mouse Genome Engineering Core Facility, University of Nebraska Medical Center, Omaha, NE 68198

[4] Department of Pharmacology and Experimental Neuroscience, College of Medicine, University of Nebraska Medical Center, Omaha, NE 68198

[5] Mathematical Biosciences Institute, Ohio State University, Columbus, OH 43210

[6] Dept of Physiology and Biophysics, University of Colorado School of Medicine, Aurora, CO 80045

Corresponding author: Helen C. Lai, Helen.Lai@utsouthwestern.edu.

Number of Figures: 9

Number of Tables: 0

Number of Multimedia: 6

Number of Extended Data Figures/Tables: 0

Number of words for Abstract: 239

Number of words for Introduction: 649

Number of words for Discussion: 1480

Conflict of Interest: The authors declare no competing financial interests.

Acknowledgments: This work was supported by R01MH120131 and R34NS121873 to K.M.D., R35HG010719 and R21GM129559 to C.B.G., and the Rita Allen Foundation, Welch Foundation I-1999-20190330, Kent Waldrep Foundation, R21NS099808 and R01NS100741 to H.C.L. We thank Lin Gan for the *Atoh1*$^{Cre/+}$ knock-in mouse, Martyn Goulding for the *Cdx2::FLPo* mouse, Susan Dymecki for the *R26*$^{LSL\text{-}FSF\text{-}TeTx}$ mouse, Mark Behlke and Sarah Jacobi from Integrated DNA Technologies for providing pre-production megamers, Rebecca Seal for the *Vglut1* ISH probe, Thomas Jessell for the *Gdnf* ISH probe, Heankel Cantu Oliveros and Wei Xu for the Lenti^{FugE}-Cre virus, Christine Ochoa and Jun Chul Kim for technical assistance, the Neuroscience Microscopy Facility which is supported by the UTSW Neuroscience Dept. and the UTSW Peter O'Donnell, Jr. Brain Institute, LifeCanvas Technologies for tissue clearing assistance, and Jane Johnson, Peter Tsai, Ariel Levine, Euiseok Kim, Abigail Person, and the Lai Lab for helpful discussions and careful reading of the manuscript.

Abstract

Proprioception, the sense of limb and body position, generates a map of the body that is essential for proper motor control, yet we know little about precisely how neurons in proprioceptive pathways are wired. Defining the anatomy of secondary neurons in the spinal cord that integrate and relay proprioceptive and potentially cutaneous information from the periphery to the cerebellum is fundamental to understanding how proprioceptive circuits function. Here, we use genetic tools in both male and female mice to define the unique anatomical trajectories of long-range direct and indirect spinocerebellar pathways as well as local intersegmental spinal circuits. We find that Clarke's column (CC) neurons, a major contributor to the direct spinocerebellar pathway, has mossy fiber terminals that diversify extensively in the cerebellar cortex with axons terminating bilaterally, but with no significant axon collaterals within the spinal cord, medulla, or cerebellar nuclei. By contrast, we find that two of the indirect pathways, the spino-lateral reticular nucleus (spino-LRt) and spino-olivary pathways, are in part, derived from cervical *Atoh1*-lineage neurons, while thoracolumbar *Atoh1*-lineage neurons project mostly locally within the spinal cord. Notably, while cervical and thoracolumbar *Atoh1*-lineage neurons connect locally with motor neurons, no CC to motor neuron connections were detected. Silencing of caudal *Atoh1*-lineage neurons results in a subtle motor impairment consistent with a defect in local proprioceptive circuitry. Altogether, we define anatomical differences between long-range direct, indirect, and local proprioceptive subcircuits that likely mediate different components of proprioceptive-motor behaviors.

Significance Statement

We define the anatomy of long-range direct and indirect spinocerebellar pathways as well as local spinal proprioceptive circuits. We observe that mossy fiber axon terminals of Clarke's column (CC) neurons diversify proprioceptive information across granule cells in multiple lobules on both ipsilateral and contralateral sides sending no significant collaterals within the spinal cord, medulla, or cerebellar nuclei. Strikingly, we find that cervical spinal cord *Atoh1*-lineage neurons form mainly the indirect spino-lateral reticular nucleus and spino-olivary tracts and thoracolumbar *Atoh1*-lineage neurons project locally within the spinal cord while only a few *Atoh1*-lineage neurons form a direct spinocerebellar tract.

61 Altogether, we define the development, anatomical projections, and some behavioral consequences of
62 silencing spinal proprioceptive pathways.

63 **Introduction**

64 Proprioception, the sense of limb and body position, is critical for generating an online state body
65 map (Sherrington, 1906; Tuthill and Azim, 2018). When proprioception is lost, gross trajectories are
66 maintained, but coordinated limb movement is impaired (Gordon et al., 1995; Abelew et al., 2000;
67 Windhorst, 2007; Akay et al., 2014). Muscle and tendon information detected by proprioceptive sensory
68 neurons are integrated by secondary neurons in the spinal cord and relayed to the cerebellum through
69 both direct and indirect spinocerebellar pathways (Oscarsson, 1965; Bosco and Poppele, 2001; Jiang et
70 al., 2015). In this study, we sought to define the precise anatomy of the proprioceptive system through
71 the spinal cord using genetic tools in mice.

72 The direct spinocerebellar pathway consists of ipsilaterally-projecting dorsal and contralaterally-
73 projecting ventral spinocerebellar tracts (DSCT and VSCT), deriving from several anatomically and
74 molecularly distinct groups of soma in diverse laminae throughout the spinal cord where they are thought
75 to convey ongoing locomotor activity (Matsushita and Hosoya, 1979; Sengul et al., 2015). A major
76 contributor to the DSCT comes from Clarke's column (CC) neurons, whose soma reside in the medial
77 aspect of the thoracic to upper lumbar spinal cord (Oscarsson, 1965; Baek et al., 2019). While SCT axons
78 terminate as mossy fiber (MF) terminals on granule cells (GCs) in the cerebellum (Arsenio Nunes and
79 Sotelo, 1985; Reeber et al., 2011), the extent to which CC neurons send axon collaterals to areas within
80 the spinal cord, medulla, or cerebellar nuclei (CN) is unclear (Ekerot and Oscarsson, 1976; Matsushita
81 and Gao, 1997; Mogensen et al., 2017; Luo et al., 2018). Such axon collaterals would be important for
82 integration with other ascending or descending pathways (Sillitoe et al., 2012; Beitzel et al., 2017).

83 Compared to the direct spinocerebellar pathways, less is known about the anatomy of the indirect
84 spino-LRt and spino-olivary (Helweg's tract) pathways. Spino-LRt neurons project ipsilaterally and
85 contralaterally to the LRt in the medulla where they are involved in posture, reaching, and grasping
86 (Alstermark and Ekerot, 2013; Jiang et al., 2015). Spino-olivary neurons reside in lamina V-VII of the

87 spinal cord and project contralaterally to the inferior olive (IO) in the medulla (Oscarsson and Sjolund,
88 1977a, b; Berkley and Worden, 1978; Swenson and Castro, 1983b, a). Neurons in the IO are thought to
89 be involved in the timing of motor commands, motor learning, and error correction (Sillitoe et al., 2012;
90 White and Sillitoe, 2017).

91 Developmentally, the basic helix-loop-helix (bHLH) transcription factor-expressing progenitor
92 domains *Atoh1* (atonal homolog 1) and the dorsal *Neurog1* (neurogenin 1) domains are reported to
93 differentiate into neurons of the direct spinocerebellar pathway (Bermingham et al., 2001; Gowan et al.,
94 2001; Sakai et al., 2012). The soma of *Atoh1*-lineage neurons reside medially, laterally, and ventrally to
95 CC neurons suggesting that CC neurons do not develop from *Atoh1*-lineage neurons, but from an
96 alternate progenitor domain (Yuengert et al., 2015). Based on the location of *Atoh1*-lineage neurons, we
97 previously hypothesized that they make other direct spinocerebellar neurons such as the lamina V-SCTs
98 or dorsal horn-SCTs (Matsushita and Hosoya, 1979; Edgley and Gallimore, 1988).

99 In this study, we sought to provide clarity to the development and anatomy of the proprioceptive
100 system using genetic labeling strategies, whole tissue clearing and imaging, and tracing tools of CC and
101 spinal cord *Atoh1*-lineage neurons. We find that CC neurons develop from a *Neurog1*, not *Atoh1*,
102 progenitor population. We also find that as a population, CC axons do not collateralize considerably to
103 any structures within the spinal cord, medulla, or CN, although they do collateralize extensively within the
104 cerebellar cortex with some axons crossing the midline within the cerebellum. Furthermore, we find that
105 cervical *Atoh1*-lineage neurons make the indirect spino-LRt and spino-olivary tracts rather than the direct
106 lamina V-SCTs or dorsal horn SCTs as originally hypothesized and that thoracolumbar *Atoh1*-lineage
107 neurons project mainly locally within the spinal cord. Altogether, we provide novel insights into the
108 development, anatomy, and function of spinal cord proprioceptive pathways.

109 **Materials & Methods**

110 *Mouse strains*

111 The following mouse strains were used: *Gdnf*$^{fRES2\text{-}CreERT2}$ (Cebrian et al., 2014)(abbreviated
112 *Gdnf*^{CreER}, JAX #024948), *Neurog1BAC-Cre* (Quinones et al., 2010)(JAX #012859), *Atoh1*$^{P2A\text{-}FLPo}$

113 (Ogujiofor et al., 2021), *Atoh1*^{Cre} knock-in (Yang et al., 2010), *R26*$^{LSL\text{-}LacZ}$ (Soriano, 1999)(JAX #003474),
114 *R26*$^{LSL\text{-}tdTom}$ (Ai14)(JAX #007914)(Madisen et al., 2010), *R26*$^{LSL\text{-}FSF\text{-}tdTom}$ (Ai65)(JAX #032864)(Madisen et
115 al., 2015), *Cdx2::FLPo* (Bourane et al., 2015), *R26*$^{LSL\text{-}FSF\text{-}TeTx}$ (Kim et al., 2009). All mice were outbred and
116 thus, are mixed strains (including C57Bl/6J, C57Bl/6N, and ICR). *Atoh1*$^{Cre/+}$ knock-in mice crossed to
117 *Cdx2::FLPo* and dual recombinase tdTomato reporter Ai65 mice were screened for "dysregulated"
118 expression as previously reported (Yuengert et al., 2015). Tamoxifen (Sigma) was injected at P7 and/or
119 P8 for the *Gdnf*^{CreER} line at 0.1 mg/g mouse using 10 mg/mL Tamoxifen dissolved in sunflower oil (Sigma)
120 with 10% ethanol. All animal experiments were approved by the Institutional Animal Care and Use
121 Committee at UT Southwestern.

122 *Tissue processing*

123 Mice are age P0 on the day of birth. Mice older than P10 were anesthetized with Avertin (2,2,2-
124 Tribromoethanol) (0.025-0.030 mL of 0.04 M Avertin in 2-methyl-2-butanol and distilled water/g mouse)
125 and transcardially perfused, first with 0.012% w/v Heparin/PBS and then 4% PFA/PBS. A dorsal or ventral
126 laminectomy exposed the spinal cord to the fixative. Spinal cords were fixed for 2 hrs and the brains
127 overnight at 4°C. Tissue was washed in PBS for at least one day and cryoprotected in 30% sucrose
128 dissolved in deionized water. Tissue was marked with 1% Alcian Blue in 3% acetic acid on one side to
129 keep orientation and were embedded in OCT (Tissue-Tek Optimal Cutting Temperature compound).
130 Tissue was sectioned using a Leica CM1950 Cryostat.

131 *Immunohistochemistry (IHC) and confocal imaging*

132 Cryosections (20-40 μm) were blocked with PBS/1-3% normal goat or donkey serum (Jackson
133 labs)/0.3% Triton X-100 (Sigma) for up to 1 hr at room temperature (RT) and incubated overnight with
134 primary antibody at 4°C. After washing 3 times with PBS, the appropriate secondary antibody (Alexa 488,
135 567, and/or 647, Invitrogen) was incubated for an hour at RT. Sections were rinsed 3 times in PBS,
136 mounted with Aqua-Poly/Mount (Polysciences Inc.), and coverslipped (Fisher). The following primary
137 antibodies and dilutions were used: 1:500 rabbit anti-dsRed (Clontech), 1:500 mouse anti-NEUN
138 (Millipore Sigma), 1:500 chicken anti-GFP (Aves), 1:5000 guinea pig anti-VGLUT1 (Millipore Sigma),

139 1:1000 guinea pig anti-VGLUT2 (Millipore Sigma), 1:100 goat anti-CHAT (Millipore Sigma), 1:200 rabbit
140 anti-PSD-95 (Invitrogen), 1:1000 rabbit anti-PV27 (Swant). Sections were referenced to the Mouse Brain
141 Atlas (Paxinos and Franklin, 2007) and Christopher Reeves Spinal Cord Atlas (Watson et al., 2009).
142 Fluorescent images were taken on a Zeiss LSM710 or LSM880 confocal microscope with an
143 optical slice of 0.5-10 μm depending on the objective used (10x air, 20x air, 40x oil, or 63x oil). Images
144 were pseudocolored using a magenta/yellow/blue, magenta/green/blue, or magenta/yellow/cyan color
145 scheme using Adobe Photoshop 2021 (Adobe) or Fiji (Schindelin et al., 2012). Images for quantitation of
146 soma size were processed in Fiji. Images were thresholded and the soma manually outlined to obtain
147 the soma area.
148 *In situ hybridization* (ISH)
149 ISH was performed as per standard protocols. Detailed protocol is available upon request. Briefly,
150 spinal cord sections (30 µm) were dried at 50˚C for 15 min. then fixed in 4% paraformaldehyde (PFA) in
151 DEPC-PBS for 20 min. at RT. The sections were washed in DEPC-PBS for 5 min. at RT before and after
152 the incubation in RIPA buffer (150 mM NaCl, 1% NP-40, 0.5% Na deoxycholate, 0.1% SDS, 1 mM EDTA,
153 50 mM Tris pH 8.0) for 60 min. Next, the sections were postfixed in 4% PFA in DEPC-PBS for 15 min at
154 RT. The sections were then washed in DEPC-water followed by acetylation (500 *μ*L of acetic anhydride
155 in 200 mL of 0.1 M RNase-free triethanolamine-HCl at pH 8.0), washed in DEPC-PBS for 5 min., and
156 prehybridized for 2 h at 60-62°C. Sections were incubated overnight at 60-62˚C with 1–2 ng/*μ*L of fresh
157 probe (*Gdnf* or *Vglut1*). A series of low and high stringency washes in 2x and 0.2x SSC as well as
158 treatment with RNaseA and RNase T1 were performed. The sections were blocked in 10% inactivated
159 sheep serum for 1 h followed by overnight incubation with 1:1000 anti-digoxygenin (DIG) antibody
160 (Roche). The sections were washed in PBT and incubated with NBT/BCIP (Roche) staining solution.
161 After the blue precipitate formed, the slides were washed in PBS and coverslipped with Aqua-Poly/Mount
162 (Polysciences Inc.) mounting media.
163 The RNAscope Fluorescent Multiplex Assay (Advanced Cell Diagnostics Inc., Hayward, CA) was
164 performed according to the manufacturer's instructions using a *Vglut1* probe (ACDBio, 416631), *Vglut2*

165 probe (ACDBio, 319171), or *Gdnf* probe (ACDBio, 421941). All incubation steps were performed in a
166 HybEZ™ II oven set to 40°C. The slides were then washed with 1x DPBS (Gibco, 14190) and incubated
167 with a 2:1 1x DPBS:Protease III for 150 sec. Slides were then washed with 1x DPBS three times and
168 incubated with the probe(s) for 2 hours. The slides were washed two times thoroughly using 1x wash
169 buffer (ACDBio, 310091) for 2 min, then incubated with Amp 1-Fl for 30 minutes. The same process
170 (washing then treatment) was repeated for Amp 2-Fl, Amp 3-Fl and Amp 4-Fl for 15, 30 and 15 minutes,
171 respectively. For antibody staining of β-galactosidase, the sections were transferred to a humidified tray
172 and blocked for 30-45 minutes in 0.25mL/slide of PBT (PBS with 0.3% Triton) containing 1% goat serum
173 (Jackson ImmunoResearch). The sections were incubated with chicken anti-β-Galactosidase antibody
174 (Abcam, 1:500) in PBT with 1% goat serum overnight at 4°C. The slides were then washed three times
175 in PBS for 10 minutes and incubated at room temperature for 1 hour with goat anti-chicken Alexa Fluor
176 488 (Life Technologies, 1:500). Slides were washed three times in PBS for 10 minutes and coverslipped
177 using 2 drops of Aqua-Poly/Mount (Polysciences, Inc.) as the mounting media.

178 *X-gal staining*

179 Slides with spinal cord sections (30 μm) were incubated in staining solution with 5mM $K_3Fe(CN)_6$,
180 5mM $K_4Fe(CN)_6$ and 1 mg/mL of X-gal (Roche) until precipitate was sufficient to visualize. Sections were
181 moved to PBS, mounted, and coverslipped.

182 *Viral Injections*

183 Mice aged P7-P8 were anesthetized using isoflurane (Henry Schein) and prepared for injections
184 into the spinal cord. The back hair was shaved and 70% ethanol and betadine (Avrio Health L.P.) applied.
185 A midline incision was made on the dorsal surface of the spinal cord. AAV9.hSyn.DIO.eGFP.WPRE.hGH
186 was injected into the lower thoracic spinal cord through the intervertebral space of P7 or P8 *Gdnf*^{Tom} mice
187 (100 nL total in 27.6 nL increments at 1-2 min intervals (Nanoject II, Drummond Scientific), 1.07 x 10^{13}
188 GC/mL, Penn Vector Core). Lenti^{FugE}-Cre was injected into the cervical or lower thoracic to lumbar area
189 of P7 *Atoh1*$^{P2A\text{-}FLPo}$*;Ai65* mice (total of 50.6 nL in 27.6 nL increments at 1-2 min intervals). Lenti^{FugE}-Cre
190 was pseudotyped with a fusion glycoprotein enabling efficient retrograde axonal transport (Kato et al.,

191 2014). To generate Lenti^{FugE}-Cre, *Cre* was sub-cloned into the third generation HIV-based lentivirus
192 vector under the control of a synapsin promoter (FSW-*Cre*). FSW-*Cre* was co-transfected into HEK293
193 cells with three packing plasmids, pMDLg/pRRE, pRSV-Rev and pCAGGS-FuG-E to generate Lenti^{FugE}-
194 Cre, which was concentrated with ultracentrifugation to 2.0 x 10^{12} Vg/mL. The incision was closed with
195 surgical glue (Henry Schein). Carprofen (5 mg/kg) was administered daily 3 days after surgery. Spinal
196 cords were harvested approximately 3 weeks after injection.

197 *CTB and FG Injections*

198 *Gdnf^{Tom}* mice were injected with 1% (w/v) of CTB-488 (left side) and CTB-647 (right side) (Thermo
199 Fisher Scientific). Mice were anesthetized with isoflurane and the area above and around the cerebellar
200 region was prepared for surgery. A midline incision of 0.75 cm and a craniectomy of approximately 1 mm
201 X 1 mm was performed. Bilateral injections at 4 sites were done at (from Bregma): rostrocaudal -5.7 and
202 -6.2 mm and at mediolateral ± 0.35 mm. At each site, several injections in 32 nL increments were
203 performed every 300 μm along the dorsoventral axis at coordinates: -1.8 and -1.5 mm deep for a total of
204 320 nL of conjugated CTB. Animals were euthanized and tissue harvested 5 days after injection.

205 Fluorogold (FG) was injected into the vermis of lobules I-V in the cerebella of *Gdnf^{Tom}*, *Atoh1^{Tom}*,
206 or *Atoh1^{Cre};Cdx2::FLPo;Ai65* mice. Mice (1-2 months old) were injected with 4% (w/v) FG solution in
207 saline (Fluorochrome). Mice were anesthetized with isoflurane and the area above and around the
208 cerebellar region was prepared for surgery. A midline incision of ~0.75 cm and a craniectomy of
209 approximately 1 mm wide by 1.5 mm long was performed. Bilateral injections at six sites were done at
210 (from Bregma): rostrocaudal -5.6 to -5.5, -5.9, and -6.25 to -6.3 mm and at mediolateral ± 0.2-0.4 mm.
211 The maximum depth at each rostrocaudal site was -2.0 mm, -2.4 mm, -1.5 mm, respectively. Multiple
212 injections were done at each site in 32 or 50.6 nL increments every 300 μm along the dorsoventral axis
213 for a total of 270-720 nL of FG on each side. Animals were euthanized and tissue harvested 7 days after
214 injection.

215 For FG injections targeting the LRt and IO, *Atoh1^{Tom}* mice (7-9 weeks old) were anesthetized with
216 isoflurane and the area above and behind the occipital region prepared for surgery. A midline incision of

217 ~1 cm was made. Neck muscles were detached from the occipital bone and retracted laterally to expose
218 the foramen magnum. A needle with a rostroventral inclination of 47° was used to advance through the
219 foramen magnum into the brainstem ~3.7 mm from dura. 32.2 nL of 1-2% (w/v) FG solution was injected
220 4-5 times 25 μm apart while retracting the pipette with an interval of 30 seconds between injections for a
221 total of 128.8-161 nL of FG. Unilateral injections were done at the following coordinates measured from
222 the most ventral aspect of the occipital crest: rostrocaudal -0.4 mm, and mediolateral ± 0.75 mm. After
223 the last injection, the needle was left in place for 3 minutes and then slowly extracted from the brainstem.
224 Animals were euthanized and tissue was harvested 7 days after injection.

225 *Whole tissue imaging*

226 Mouse hindbrain and spinal cords were processed following the SHIELD protocol (Park et al.,
227 2018). Tissues were cleared with SmartClear II Pro (LifeCanvas Technologies, Cambridge, MA) for
228 several days, mounted in a gel of 0.9% agarose in EasyIndex (LifeCanvas Technologies), and then
229 incubated in EasyIndex for refractive index matching. Tissues were imaged at 3.6X using a SmartSPIM
230 light sheet microscope (LifeCanvas Technologies). Spinal cords and hindbrains of three mice marking
231 CC were used for quantitation of the MF/cell body ratio: one *Gdnf*^{Tom} mouse (female, P23) and two
232 *Gdnf*^{Tom};*Cdx::FLPo;Ai65* mice (one male, one female, P28). Mice were imaged with 1.8 μm x 1.8 μm x 2
233 μm sampling (X, Y, and Z, respectively). The total number of 2 μm image slices for each sample was as
234 follows: spinal cord (1500, 3300, 2400 slices) and hindbrain (2700, 3000, 3300 slices) for the *Gdnf*^{Tom},
235 *Gdnf*^{Tom};*Cdx::FLPo;Ai65* male, *Gdnf*^{Tom};Cdx::FLPo;Ai65 female mouse, respectively. One
236 *Atoh1*^{Tom};*Cdx::FLPo;Ai65* mouse spinal cord and hindbrain was cleared (male, P30). The hindbrain was
237 imaged as described above (4800 slices). The spinal cord was imaged with a 15x objective with 0.41 μm
238 x 0.41 μm x 2 μm sampling (900 slices). All hindbrain and spinal cord samples were cut to less than 2.2
239 cm to fit in the imaging chamber. Movies were made in arivis Vision4D 2.12.6. Maximum intensity
240 projections (MIPs) were processed using Fiji (Schindelin et al., 2012).

241 *Behavioral test - Rotarod*

242 Rotarod was performed at 8-13 weeks of age. All testers were blind to genotype. Mice were
243 acclimated to the testing room for 0.5-1 hr on day of testing. All mice were genotyped for appropriate
244 alleles using previously published protocols for *Atoh1*^{Cre}, *Cdx::FLPo*, and *R26*$^{LSL\text{-}FSF\text{-}TeTx}$ (Kim et al., 2009;
245 Yang et al., 2010; Bourane et al., 2015). Mice were placed on an accelerating rotarod (IITC Life Science
246 Series 8, Woodland Hills, CA) from 4 to 40 RPM over 5 min. Four trials were performed each day for two
247 days with at least a 15 min wait time between trials.

248 *Experimental Design and Statistical Tests*

249 The mossy fiber (MF) to cell body ratio (Fig. 3K) was counted from three cleared spinal cords and
250 hindbrains. Cells bodies in the spinal cord and MFs in the cerebellar cortex were counted from 100 μm
251 MIP images of cleared tissue. The ratio calculated is an estimate given that it is impossible to accurately
252 count all the cell bodies and MF terminals and there are many opportunities for over- or undercounting.
253 For example, although cell bodies and mossy fibers were counted only when they could be discretely
254 identified, some MF terminals might appear as two MF terminals, when they in fact come from the same
255 MF. As an example of undercounting, cell bodies and mossy fibers may overlap in the z axis of the 100
256 μm MIP and may be counted as one instead of several. Altogether, cell bodies and MFs were counted to
257 get an estimate rather than an exact count of the MF/cell body ratio.

258 For the mapping of thoracolumbar CC MF terminals in the cerebellum (Fig. 4H-H'''', J-J'''', L-L'''',
259 N, P, R), confocal images of 30 μm cryosections were analyzed in Fiji using the ROI Manager to label
260 individual MF terminals and the SlideSet PlugIn to export the ROIs as a .svg file (Schindelin et al., 2012;
261 Nanes, 2015). These mapped MF terminals were then overlaid on a traced drawing of the confocal image
262 in Adobe Illustrator 2021.

263 All data and graphs were processed in Microsoft Excel 2015 and GraphPad Prism 9. Details of
264 the number of sections counted and sex of the mice are given in the Results section. Mean ± SEM is
265 reported throughout the manuscript. Statistical tests used are detailed in the Results and/or Figure
266 Legends.

267 **Results**

268 *Clarke's column is the major direct spinocerebellar pathway in mice.*

269 To assess the spinocerebellar system in mice, we identified genetic tools that reproducibly label
270 spinal cord neurons and evaluated their contribution to the spinocerebellar system using a combination
271 of retrograde and anterograde tracing. Previously, we found that the *Atoh1*-expressing progenitor
272 population that makes dorsal interneuron 1 (dI1) neurons, although implicated in making spinocerebellar
273 neurons developmentally (Bermingham et al., 2001; Gowan et al., 2001; Sakai et al., 2012), rarely made
274 CC neurons, which are the major source of the DSCT (Fig. 1A, note the absence of TOM^{+} cells in the CC
275 area of *Atoh1*-lineage traced neurons, *Atoh1*^{Cre};*R26*$^{LSL\text{-}tdTom}$ (Ai14), abbreviated *Atoh1*^{Tom})(Madisen et al.,
276 2010; Yang et al., 2010; Yuengert et al., 2015). Therefore, we sought to identify the progenitor population
277 that gives rise to CC neurons. Evidence from spinal cord development suggested that the neighboring
278 *Neurog1*-expressing progenitor population that makes dI2 neurons also project to the cerebellum
279 (Avraham et al., 2009; Sakai et al., 2012). Because there are no uniquely specific molecular markers for
280 the dI2 population, we traced the lineage of the entire *Neurog1* population, which includes dI2 neurons
281 and ventral domains, using a transgenic *Neurog1BAC-Cre* strain crossed to a *R26*$^{LSL\text{-}LacZ}$ reporter mouse
282 (Fig. 1A)(Soriano, 1999; Quinones et al., 2010). Large CC cells residing in the medial thoracic spinal cord
283 colocalize with vesicular glutamate transporter 1 (*Vglut1*) mRNA, a marker for CC (Fig. 1A, B)(Llewellyn-
284 Smith et al., 2007; Malet et al., 2013; Yuengert et al., 2015). Therefore, CC neurons come from a
285 *Neurog1*-lineage (dI2 or ventral lineages), but not the *Atoh1*-lineage.

286 Next, we further characterized molecular tools that label CC neurons. As previously described,
287 CC neurons are marked by glial derived nerve growth factor (*Gdnf*) and *Vglut1* mRNA (Fig. 1B)(Llewellyn-
288 Smith et al., 2007; Hantman and Jessell, 2010; Malet et al., 2013). We found that *Gdnf* is transiently
289 expressed from E18.5-P10 (data not shown) and that *Gdnf* and *Vglut1* mRNA completely overlap at P10
290 (Fig. 1C, arrowheads). Furthermore, CC neurons that are retrogradely labeled with Fluorogold (FG)
291 injected into the anterior zone (AZ, lobules I-V) of the cerebellum, colocalized with *Vglut1* mRNA (Fig.
292 1D, arrowheads). A subset of CC neurons is labeled using a *Gdnf*$^{IRES2\text{-}CreERT2/+}$ mouse line crossed to a
293 CRE-dependent tdTomato reporter (Ai14) (abbreviated *Gdnf*^{Tom} from here on)(Fig. 1D, arrows)(Hantman

294 and Jessell, 2010; Cebrian et al., 2014). Lastly, we found that CC neurons also express vesicular
295 glutamate transporter 2 (*Vglut2*)(Fig. 1E, arrowheads). We used the *Gdnf*$^{IRES2\text{-}CreERT2/+}$ mouse line
296 (abbreviated *Gdnf*^{CreER} from here on) for the remainder of the study due to its specific labeling of CC
297 neurons.

298 To understand the relationship of the direct spinocerebellar system to our two CRE mouse lines
299 (*Gdnf*^{CreER} and *Atoh1*^{Cre}), we used both anterograde (Fig. 1F-I) and retrograde (Fig. 1J-P) tracing
300 strategies to and from the cerebellum. To identify ascending projections from the spinal cord, we used
301 an intersectional strategy to restrict labeling of neurons to regions caudal of cervical 4
302 (C4)(*Cdx2::FLPo*)(Bourane et al., 2015). As expected, we found that CC neurons (*Gdnf*^{CreER}*; Cdx2::FLPo;*
303 *Ai65*) terminate as mossy fibers (MF) in the AZ of the cerebellum and express VGLUT1^{+} (VG1) and
304 VGLUT2^{+} (VG2) presynaptic markers (Fig. 1F-F'''). However, labeling of caudal *Atoh1*-lineage neurons
305 (*Atoh1*^{Cre}; *Cdx2::FLPo*; *Ai65*) had very few MF terminals in the AZ, although they were VG1^{-} and VG2^{+},
306 consistent with a non-Clarke's spinocerebellar population and a previous report that spinocerebellar
307 neurons are mainly VG2^{+} with some VG1^{+} MF terminals (Gebre et al., 2012; Yuengert et al., 2015)(Fig.
308 1G-G'''; Quantitated in Fig. 1H, in the AZ, 2447 ± 624 *Gdnf*^{CreER}*; Cdx2::FLPo; Ai65* (n=3, 2 females (F):1
309 male (M)) vs. 690 ± 213 *Atoh1*^{Cre}; *Cdx2::FLPo*; *Ai65* (n=3, 1F:2M), t-test p=0.056, 3 comparable
310 sections/n; MF terminals in lobules VIII/IXa are similar, 262 ± 75 *Gdnf*^{CreER}*; Cdx2::FLPo; Ai65* vs. 182 ±
311 21 *Atoh1*^{Cre}; *Cdx2::FLPo*; *Ai65,* 1 comparable section/n; ages P27-67). The difference in MF terminals is
312 striking given that *Atoh1*-lineage neurons have many more soma per section throughout the rostral-
313 caudal axis compared to CC neurons (Fig. 1I, *Gdnf*^{CreER}*; Cdx2::FLPo; Ai65* (n=3, 2F:1M, 4 sections
314 counted per region per n), *Atoh1*^{Cre}; *Cdx2::FLPo*; *Ai65* (n=2, 1F:1M, 3-4 sections counted per region per
315 n)), suggesting there are many more MF terminals per CC soma in the spinal cord compared to caudal
316 *Atoh1*-lineage neurons.

317 Consistent with our anterograde tracing findings, we found that retrograde labeling of
318 spinocerebellar neurons colocalized with CC neurons, but few *Atoh1*-lineage neurons (Fig. 1J-P). FG
319 was injected into the cerebella of *Gdnf*^{Tom} or *Atoh1*^{Tom} mouse strains targeting the AZ where

320 spinocerebellar neurons are known to project (Fig. 1 J, K, N)(Arsenio Nunes and Sotelo, 1985; Bosco
321 and Poppele, 2001; Reeber et al., 2011). Overall, FG retrograde tracing from all injections were similar
322 with 261 ± 39 total FG$^+$ cells in injections of *Gdnf^{Tom}* (n=3, 1F:2M, ages P38-40, counts from 5 sections
323 per spinal cord region per n) and 228 ± 32 total FG$^+$ cells in injections of *Atoh1^{Tom}* (n=4, 3F:1M, ages
324 P39-40, counts from 5 sections per spinal cord region per n)(Fig. 1L, O shows total FG cells in each
325 spinal cord region). Overall, CC is the most abundantly labeled spinocerebellar projection making up 43-
326 47% of all retrogradely-labeled FG neurons in the spinal cord (Fig. 1M, P). The next most abundant
327 areas of spinocerebellar neurons along the rostral-caudal axis are those in the central cervical (CeCv)
328 nucleus (Cummings and Petras, 1977; Wiksten, 1987; Popova et al., 1995) and cells dorsal or ventral of
329 the central canal in the thoracolumbar areas (Fig. 1K', N', top and lower panels; L-M, O-P), which
330 correspond to LV-SCT, LVII-SCT, LVIII-SCT, and spinal border cells (Baek et al., 2019). Notably,
331 spinocerebellar neurons in the CeCv and thoracolumbar areas (excluding CC) are rarely colabeled with
332 *Gdnf^{Tom}* or *Atoh1^{Tom}* neurons (Fig. 1L-M, O-P) indicating that genetic labels for these spinocerebellar
333 neurons and their developmental origins have yet to be determined. *Gdnf^{Tom}* makes up 12 ± 2% of the
334 FG$^+$ CC neurons out of all FG$^+$ neurons in the spinal cord and therefore labels ~ 29 ± 1% of CC neurons.
335 The remaining approximately 70% of unlabeled CC neurons in the *Gdnf^{Tom}* line could be due to the
336 restricted time point at which tamoxifen was injected (P7-P8), incomplete CRE recombination, or
337 represent a unique subset of CC neurons. *Atoh1^{Tom}* makes up 3 ± 1% of the FG$^+$ CC neurons out of all
338 FG$^+$ neurons in the spinal cord and therefore labels ~ 6 ± 1% of CC neurons, consistent with our previous
339 findings that *Atoh1*-lineage neurons make up very few CC neurons (Yuengert et al., 2015). Significantly,
340 only 4 ± 1% of all spinocerebellar (FG$^+$) neurons projecting to the AZ in the entire spinal cord are *Atoh1*-
341 lineage neurons (FG$^+$TOM$^+$). Altogether, our data suggest that CC makes up a majority of spinocerebellar
342 neurons projecting directly to the AZ, while *Atoh1*-lineage neurons make up very few direct
343 spinocerebellar neurons. Using our genetic tools, we then proceeded to determine the precise anatomy
344 of both CC and *Atoh1*-lineage projections.
345 *Anatomical trajectories of CC neurons.*

346 We used the *Gdnf*^{Tom} line to meticulously trace axonal trajectories of CC neurons to the
347 cerebellum and found that the axons cross within the cerebellum and terminate almost exclusively as
348 MFs on granule cells. We found that CC MF terminals in the cerebellum terminate in the vermis of lobules
349 II-V, VIII, IXa, and the copula pyramidis (Cop) (Fig. 2A-C), consistent with the termination locations of
350 spinocerebellar neurons from previous pan-anterograde tracing studies (Arsenio Nunes and Sotelo,
351 1985; Bosco and Poppele, 2001; Apps and Hawkes, 2009; Reeber et al., 2011). In addition, the three
352 parasagittal stripes in lobule III on both sides of the midline closely matched those found in anterograde
353 tracing studies from the thoracic and lumbar spinal cord (Fig. 2A, B)(Ji and Hawkes, 1994; Reeber et al.,
354 2011). However, while CC axons are known to travel rostrally ipsilaterally in the lateral funiculus of the
355 spinal cord (Oscarsson, 1965 and see Movie 1), we found that several axons appeared to cross the
356 midline within the cerebellum (Fig. 2D, E), suggesting that CC axons terminate both ipsilaterally and
357 contralaterally in the cerebellar cortex, which has been seen in single-cell reconstructions (Luo et al.,
358 2018). To test whether CC axons from a given CC cell terminates on both sides of the cerebellum, we
359 injected two different Cholera Toxin subunit B (CTB)-conjugated fluorophores (CTB-488 and CTB-647)
360 into the left and right sides of the cerebellum (Fig. 2F, G). We found retrogradely labeled cells in CC of
361 the spinal cord that took up both tracers (Fig. 2H, arrows and arrowheads), some of which were colabeled
362 with *Gdnf*^{Tom} (Fig. 2H, arrows). Approximately 30% of the terminals from CC neurons that innervate the
363 injection area are from the contralateral side (% ipsi and contra CTB-488/total CTB-488: 74 ± 4% and 26
364 ± 4%, respectively; % ipsi and contra CTB-647/total CTB-647: 70 ± 5% and 30 ± 5%, respectively, n=3,
365 2F:1M, 8 sections/n, age P65-95). This could mean that only 30% of CC neurons cross or that all of them
366 cross, but only some CC neurons have enough terminations on the contralateral side to allow for sufficient
367 CTB uptake. Therefore, CC neurons project ipsilaterally within the spinal cord, but send collaterals to
368 both ipsilateral and contralateral sides within the cerebellum.

369 Strikingly, we found that CC axons do not make significant axon collaterals within the spinal cord,
370 medulla, or to the cerebellar nuclei, a feature typical of other MF tracts, but has been ambiguous for the
371 spinocerebellar system (Fig. 3A-H')(Matsushita and Ikeda, 1970; Matsushita and Gao, 1997; Mogensen

372 et al., 2017). In three separate samples, we found no axon terminations in the Medial (Med), Interpositus
373 (Int), or Lateral (Lat) cerebellar nuclei (CN). Areas near the cerebellar nuclei that had TOM$^+$ signal came
374 from axons of passage and not synaptic terminations (TOM$^+$ axons are VG1$^-$ or VG2$^-$ (Fig. 3A', A'', D',
375 D'')). Furthermore, we find no seeming axon collaterals within the spinal cord (Movie 1), nor do we find
376 significant synaptic terminations in the LRt or nucleus X, as was reported previously for some CC neurons
377 (Fig. 3G-H')(Luo et al., 2018). Some synaptic terminals can be seen in the LRt (Fig. 3G', arrow), but the
378 axons mainly appear to be coursing by the LRt. In summary, our genetic studies of CC neurons show
379 that these glutamatergic neurons terminate bilaterally in the cerebellar vermis, but do not make significant
380 axon collaterals to the spinal cord, medulla, or cerebellar nuclei.

381 *Diversification of proprioceptive information through CC neurons.*

382 To obtain a three-dimensional view of CC trajectories, we chemically cleared the spinal cords and
383 hindbrains of *Gdnf^{Tom}* and *Gdnf^{CreER};Cdx2::FLPo*; *Ai65* mice (Movies 1-2). Because *Gdnf* is also
384 expressed in smooth and skeletal muscle (Trupp et al., 1995; Suzuki et al., 1998; Rodrigues et al., 2011),
385 they are prominently labeled with TOM in these samples. In the spinal cord (Movie 1), the CC soma can
386 be seen straddling the midline, while their axons extend to the lateral funiculus (LF) where they make a
387 90° turn heading rostrally to the cerebellum. Axons in the inferior cerebellar peduncle are seen traveling
388 directly to the cerebellum (Movie 2).

389 A feature that was readily apparent from the cleared specimens was the sheer number of MF
390 terminals in the cerebellum indicating an immense diversification of proprioceptive information coming
391 from CC axons (Fig. 3I-K). We counted the number of MF terminals per CC soma in the cerebella and
392 spinal cords of the three cleared samples. From these counts, we estimate that there are 71.9 ± 6.1 MF
393 terminals in the entire cerebellum for each CC soma (Fig. 3K, orange bar). The MFs terminate largely in
394 vermis I-III (34.6 ± 3.0 MF/soma ratio), IV/V (24.7 ± 2.1), VIII (4.6 ± 0.7), IXa (0.6 ± 0.2), and the copula
395 (7.2 ± 1.3)(n=3, 2F:1M, ages P23-28), consistent with the distribution seen in cryosections (Fig. 2A-C).
396 The large ratio of MFs to CC soma suggests that CC information is widely distributed within the
397 cerebellum. Furthermore, the proprioceptive information coming into CC neurons require surprisingly few

398 CC neurons to relay that information to the cerebellum. We counted a range of 486-816 CC neurons in
399 the three spinal cords, which represents around 29% or less of all CC neurons labeled in the *Gdnf*^{Tom} and
400 *Gdnf*^{CreER}*;Cdx2::FLPo*; *Ai65* mouse models for an estimated 1,620 to 2,720 CC neurons in the mouse
401 spinal cord. This suggests that most of the mouse proprioceptive direct spinocerebellar system comes
402 from roughly a couple thousand neurons.

403 Next, we wanted to test whether CC neurons from a restricted area of the spinal cord terminate
404 in clustered or diverse locations in the cerebellum. If a given CC neuron sends MFs terminals to one
405 discrete localized area of the cerebellum, this would suggest that proprioceptive information exists as a
406 traditional homunculus in the cerebellum. However, if a given CC neuron sends MF terminals to multiple
407 areas of the cerebellar cortex, this would provide an anatomical substrate for the fractured somatotopic
408 map that has been detected electrophysiologically (Shambes et al., 1978), where body parts are
409 represented in discontinuous patches across the cerebellum (Manni and Petrosini, 2004; Apps and
410 Hawkes, 2009). To label CC neurons specifically in the thoracolumbar area, we injected AAV9-Syn-DIO-
411 EGFP into *Gdnf*^{Tom} mice (Fig. 4A). Our injections labeled CC neurons on both sides of the spinal cord
412 (Fig. 4B, B', arrows) and largely the lower thoracolumbar spinal cord (Fig. 4G, I, K, M, O, Q)(counts for
413 GFP^{+} infection in the spinal cord are from 15-16 sections per spinal cord region). We found that
414 thoracolumbar CC neurons targeted multiple lobules (II-V, VIII)(GFP^{+} (green) and GFP^{+}TOM^{+} (yellow),
415 Fig. 4H-H''', J-J''', L-L''', N, P, R, coronal and sagittal sections, n=3 each, 1F:2M for coronal sections,
416 2F:1M for sagittal sections). Although there were discrete areas that did not contain GFP^{+} cells
417 (arrowheads, Fig. 4H-H''', J-J''', L-L'''), GFP^{+} cells were found over multiple lobules indicating that CC
418 axonal projections from the thoracolumbar spinal cord terminate throughout the cerebellar cortex,
419 consistent with a discontinuous somatotopic map. Examples of GFP^{+} (green, arrowheads) and
420 GFP^{+}TOM^{+} (white, arrows) MF terminals in lobules III and VIII in both coronal and sagittal sections are
421 shown (Fig. 4S, T). In addition to terminating across several lobules, we found multiple examples of single
422 axons terminating at regular intervals (50-80 μm) within a GC layer, which has been reported anecdotally
423 in the literature (Reeber et al., 2011; Houck and Person, 2015; Gilmer and Person, 2017; Luo et al.,

424 2018), indicating that a single CC neuron synapses on several GCs (Fig. 4C-F). Interestingly, an
425 individual GC is approximately 40-50 μm from dendrite to dendrite (Gray, 1961; Eccles et al., 1967; Jakab
426 and Hamori, 1988; Huang et al., 2013). Therefore, individual MF axons from a single CC neuron likely
427 do not synapse on the same GC suggesting that GCs are multimodal encoders at the single cell level
428 (Marr, 1969; Albus, 1971). Overall, we find that CC neurons arborize extensively within the cerebellar
429 cortex, reaching targets over multiple lobules, rather than in clustered locations.

430 *Atoh1-lineage neurons make the spino-LRt and spino-olivary tracts*.

431 Given that *Atoh1*-lineage neurons made few direct spinocerebellar neurons, we sought to identify
432 where in the hindbrain *Atoh1*-lineage axons project. We pursued an intersectional genetic strategy to
433 restrict somatic labeling to caudal *Atoh1*-lineage neurons (*Atoh1^{Cre}; Cdx2::FLPo; Ai65*)(Fig. 5A). Most
434 prominently, we found dense projections of caudal *Atoh1*-lineage neurons in the lateral reticular nucleus
435 (LRt) and inferior olive (IO) (Fig. 5E-H''). To identify whether caudal *Atoh1*-lineage axons synapse on
436 localized areas of the LRt and IO, we injected FG into the cerebellar AZ (Fig. 5A-B), which retrogradely
437 labeled LRt MF and IO CF cell bodies. We found that caudal *Atoh1*-lineage axons target almost the
438 entirety of the LRt and restricted areas of the IO (dorsal fold of the dorsal accessory olive (dfDAO), dorsal
439 accessory olive (DAO), subnucleus a of the caudal medial accessory olive (cMAO^{a}), subnucleus b of
440 cMAO (cMAO^{b})(Fig. 5E'-H'). Consistent with our findings, anterograde tracing in rats reports that the
441 spino-olivary tract terminates in the DAO, cMAO^{a}, and cMAO^{b} (Swenson and Castro, 1983a; Matsushita
442 et al., 1992; Oldenbeuving et al., 1999). Caudal *Atoh1*-lineage axons colocalize with the presynaptic
443 marker VG2 and are in close apposition to FG labeled neurons in the LRt and IO indicative of synaptic
444 connections (arrows, Fig. 5I-J, Movies 5 and 6). Axon terminations in the LRt and IO were verified in four
445 caudal *Atoh1*-lineage mice. Moreover, TOM^{+} terminals in a cleared brain of *Atoh1^{Cre}; Cdx2::FLPo; Ai65*
446 mice are quite dense in the LRt and IO (Movie 4). Altogether, we find that spinal cord *Atoh1*-lineage
447 neurons make the spino-LRt and spino-olivary tracts.

448 In the caudal *Atoh1*-lineage mice, a few places of expression are worth noting. First, the sensory
449 neurons misexpress tdTomato and their axons can be seen terminating in the dorsal horn of the cleared

450 spinal cord (Movie 3). *Atoh1* is not known to be expressed in sensory neurons and we do not see sensory
451 neurons labeled in *Atoh1*$^{P2A\text{-}FLPo}$ mice, whose expression overlaps quite well with the *Atoh1*^{Cre} knockin
452 mouse for spinal cord interneurons (data not shown and Ogujiofor et al., 2021). Therefore, the sensory
453 neuron labeling is due to misexpression of the CRE recombinase in sensory neurons. As a result, axons
454 from sensory neurons going to the gracile, cuneate, and external cuneate nuclei can be seen in the
455 cleared brain of *Atoh1*^{Cre}*; Cdx2::FLPo; Ai65* mice (Movie 4). Second, we find sparse ectopic labeling of
456 *Atoh1*-lineage spinal vestibular (SpVe) soma in the hindbrain (Fig. 5C)(Rose et al., 2009). SpVe neurons
457 send descending projections to the spinal cord (Liang et al., 2015), therefore, we do not expect that this
458 sparse ectopic labeling interferes with our analysis of ascending projections from caudal spinal cord
459 *Atoh1*-lineage neurons. Lastly, we detect some TOM^{+} axons in the lateral parabrachial nucleus (LPB) in
460 *Atoh1*^{Cre}*; Cdx2::FLPo; Ai65* mice (TOM^{+}VG2^{+}, Fig. 5D-D'). Further studies are needed to determine
461 exactly from where in the spinal cord these LPB projections originate and if they are truly *Atoh1*-lineage
462 neurons or ectopic expression.

463 *Spino-LRt and spino-olivary axonal projections originate from cervical Atoh1-lineage neurons.*

464 We pursued both retrograde and anterograde tracing strategies to determine which caudal *Atoh1*-
465 lineage neurons contribute to the spino-LRt and spino-olivary tracts. In four different FG injections
466 targeting the LRt and IO in *Atoh1*^{Tom} mice, we found that the retrogradely labeled *Atoh1*-lineage cells
467 resided mainly in the cervical to upper thoracic areas (Fig. 6A-G, light purple (left side) and light blue
468 (right side) FG^{+}TOM^{+} cells quantitated in B, C, E, F; n=4, 3F:1M, 5 sections counted per spinal cord
469 region, 7-9 weeks old). *Atoh1*-lineage neurons have previously been described as clustering into lateral
470 and medial populations, which are thought to make up ipsilaterally- and contralaterally-projecting
471 populations, respectively (Bermingham et al., 2001; Wilson et al., 2008; Yuengert et al., 2015).
472 Retrogradely labeled neurons from the LRt and IO colocalized with both the lateral (Fig. 6D', G') and
473 medial (Fig. 6G'') *Atoh1*-lineage neurons. Because of the spread of the FG to both the LRt and IO, the
474 precise ipsilateral or contralateral projections from either tract was not clear, but *Atoh1*-lineage neurons
475 both ipsilateral (Fig. 6G') and contralateral (Fig. 6G'') to the injection site were retrogradely labeled. Given

476 the large number of neurons retrogradely labeled from the LRt and IO that are not *Atoh1*-lineage suggests
477 that there are many other progenitor domains and cell types that contribute to these tracts (Alstermark
478 and Ekerot, 2013; Azim et al., 2014; Pivetta et al., 2014; Jiang et al., 2015; Choi et al., 2020).

479 To identify the axonal projection targets of cervical *Atoh1*-lineage neurons, we pursued an
480 intersectional strategy injecting Lenti$^{FugE\text{-}Cre}$ into the cervical area of *Atoh1*$^{P2A\text{-}FLPo}$ mice crossed to an
481 intersectional tdTomato reporter (*Ai65*) (Fig. 6H). In one mouse, the infected neurons were restricted to
482 the right spinal cord (Fig. 6I-J) and in another mouse, the infected cells were on both the left and right
483 sides (Fig. 6 L, M)(n=2 male mice, 8-15 sections counted per spinal cord region, P30). In the mouse with
484 the injection restricted to the right side, prominent axons were seen in the right LRt and the TOM$^+$
485 terminations express VG2 (Fig. 6K-K'), suggesting that minimally, the spino-LRt *Atoh1*-lineage neurons
486 are ipsilaterally-projecting. In the other mouse that had TOM$^+$ cells on both sides of the spinal cord, likely
487 due to the virus being taken up by contralaterally-projecting *Atoh1*-lineage neurons, we found axonal
488 terminations in the right LRt and right cMAOb that were VG2$^+$ and closely apposed to the postsynaptic
489 density protein (PSD-95$^+$), suggesting that these are functional excitatory synapses (Fig. 6N-O'',
490 TOM$^+$VG2$^+$, white arrowheads; PSD95$^+$, grey arrowheads).

491 We next examined the local inputs and outputs of cervical *Atoh1*-lineage neurons. We had
492 previously shown that thoracolumbar *Atoh1*-lineage neurons receive proprioceptive input (Yuengert et
493 al., 2015). Here, we found that both medial and lateral *Atoh1*-lineage neurons in the cervical area (TOM$^+$)
494 have processes closely apposed to VG1$^+$ and Parvalbumin (PV$^+$) synapses indicative of proprioceptive
495 afferents (Fig. 6Q-Q'). Similar to our previous results for the thoracolumbar *Atoh1*-lineage neurons
496 (Yuengert et al., 2015), we were able to visualize axo-somatic synapses for the medial population (Fig.
497 6Q, VG1$^+$PV$^+$, white arrowhead), but we were unable to identify axo-somatic synapses on the lateral
498 population. We could only find VG1$^+$PV$^+$ afferents passing near TOM$^+$ processes in the vicinity of the
499 lateral soma (Fig. 6Q', VG1$^+$PV$^+$, white arrowhead; TOM$^+$, grey arrowhead). Lastly, we found that the
500 axons of sparsely labeled cervical *Atoh1*-lineage neurons made synapses on motor neurons (MNs)(Fig.

501 6R-R'). Altogether, we found that cervical *Atoh1*-lineage neurons can receive proprioceptive input and do
502 indeed project to the LRt and IO as well as locally to MNs in the cervical spinal cord.

503 *Thoracolumbar Atoh1-lineage neurons project locally.*

504 We next examined whether sparsely labeled thoracolumbar *Atoh1*-lineage neurons send axonal
505 projections to the medulla or cerebellum. Using the same intersectional injection strategy except with the
506 Lenti$^{FugE\text{-}Cre}$ targeted to the right thoracolumbar spinal cord (light blue), we again found several cell bodies
507 on the contralateral side labeled (Fig. 7B, 786 ± 20 cells, right side vs. 598 ± 223 cells, left side; n=4,
508 3F:1M, total number of cells infected was estimated from counts of 20% of each spinal cord region),
509 which is likely due to the virus being taken up by axons of passage projecting contralaterally (Fig. 7C,
510 axons labeled in the right ventral funiculus (Rt VF)(light blue arrowhead)). Most of the cell bodies labeled
511 were in the thoracolumbar area (Fig. 7D)(cell bodies counted from 13-30 sections per spinal cord region).
512 Strikingly, we found that axons in the right ventral and lateral funiculi (VF, LF) decreased both rostrally
513 and caudally, suggesting that most of these axons are local projections (Fig. 7E)(axons counted from the
514 right and left LF and VF from one section/spinal cord region) and that few thoracolumbar *Atoh1*-lineage
515 neurons project to the LRt, IO, and cerebellar cortex.

516 Interestingly, the neurons labeled on the left side of the spinal cord, contralateral to the injected
517 side, were located more dorsolaterally than expected for the medial *Atoh1*-lineage population that is
518 known to project contralaterally (Fig. 7C, purple arrows)(Bermingham et al., 2001; Wilson et al., 2008;
519 Yuengert et al., 2015). This observation prompted us to characterize the distribution and cell soma size
520 of infected *Atoh1*-lineage neurons (Fig. 7F-H'). In the spinal cord areas of peak infection (T11-13, L1-3,
521 and L4-6), we found that medial, lateral, and the ill-described ventral *Atoh1*-lineage populations on both
522 sides of the spinal cord were labeled (Fig. 7F-H, n=4, 3-6 sections/n). Quantitation of the soma area
523 found no size differences between the lateral, medial, and ventral population on either side (one-way
524 ANOVA of clusters that had n > 5 cells). We believe that the cells infected on the left side are labeled
525 through their contralaterally-projecting axons that take up the virus on the right side. This suggests that
526 at least a subset of lateral *Atoh1*-lineage cells can also project contralaterally. Indeed, imaging of some

527 of the neurons on the left side shows processes projecting both ventromedially and dorsolaterally (inset
528 in Fig. 7F, arrows), suggesting that these neurons could project both ipsilaterally and contralaterally.
529 While it is possible that cells labeled on the left side are due to diffusion of the virus across the midline,
530 we would have expected the lateral *Atoh1*-lineage neurons in this scenario to project ipsilaterally and
531 therefore, there should be almost equal numbers of axons in the left and right LF given that the number
532 of soma on each side is similar. However, the number of axons in the left LF are low compared to the
533 right LF (Fig. 7E). Therefore, we surmise that the neurons infected on the left side are contralaterally-
534 projecting lateral *Atoh1*-lineage cells, a subset of which could also project ipsilaterally.

535 Because of the dense ventral projections in our sparsely labeled *Atoh1*-lineage neurons (Fig. 7C,
536 T11-13 and L1-3), we asked whether thoracolumbar *Atoh1*-lineage neurons also synapse on motor
537 neurons. Similar to the cervical *Atoh1*-lineage neurons, we found in all four injections a high density of
538 $TOM^{+}VG2^{+}$ puncta (arrowheads, Fig. 7I-I') near and some very closely apposed to $CHAT^{+}$ motor neurons
539 (arrowhead, Fig. 7I''). Some of these $TOM^{+}VG2^{+}$ puncta might be axo-dendritic synapses (Fig. 7I',
540 arrowheads), while only a few axo-somatic contacts are detected (Fig. 7I''). Thus, we find that
541 thoracolumbar *Atoh1*-lineage neurons primarily project locally, where they synapse onto motor neurons,
542 with few neurons projecting to higher brain regions.

543 *Expression of a silencing allele in caudal Atoh1-lineage neurons leads to a subtle motor defect.*

544 To understand how caudal *Atoh1*-lineage neurons affect motor behavior, we expressed GFP-
545 tetanus toxin light chain fusion protein (TeTx), which should inhibit vesicle neurotransmission (Kim et al.,
546 2009), in these neurons using an intersectional genetic strategy (*Atoh1*^{Cre}*;Cdx2::FLPo;R26*$^{LSL\text{-}FSF\text{-}TeTx}$)(Fig. 8A). In caudal *Atoh1*-lineage neurons heterozygous for the TeTx allele, we found a subtle motor
548 phenotype. We only analyzed mice heterozygous for the TeTx allele because the *Atoh1* gene is close to
549 the *ROSA* locus on chromosome 6 and thus, homologous recombination occurs too infrequently to get
550 homozygosity at the *ROSA* locus along with the *Atoh1*^{Cre} allele. Caudal *Atoh1*-lineage neurons
551 expressing the TeTx allele fell off the rotarod sooner compared to controls (Fig. 8B, p=0.0255 for a main
552 effect due to genotype).

553 The way that the *R26*$^{LSL\text{-}FSF\text{-}TeTx}$ mouse was designed, CRE recombinase expression allows for
554 mCherry expression while CRE and FLPo recombinase allows for expression of the GFP-TeTx fusion
555 protein (Kim et al., 2009). We performed immunofluorescence and immunohistochemistry with three
556 different GFP antibodies, but were unable to verify expression of the GFP-TeTx fusion protein. Instead,
557 we were able to verify that mCherry was expressed in the upper cervical areas of the spinal cord where
558 *Atoh1*^{Cre} is expressed, but not Cdx2*::FLPo* (Fig. 8C-C'). Correspondingly, in the lumbar area of the spinal
559 cord where both *Atoh1*^{Cre} and *Cdx2::FLPo* are expressed, the mCherry is no longer expressed indicating
560 that the FLPo recombinase had recombined out the mCherry. All twenty-two heterozygous mice
561 expressing TeTx were confirmed to lack mCherry expression in the lumbar compared to cervical spinal
562 cord.

563 **Discussion**

564 In this study, we define the anatomy of proprioceptive spinal pathways and find surprising features
565 of these ascending projections (summarized in Fig. 9). We find that CC neurons avoid significant
566 collateralization within the spinal cord, medulla, and CN, although they do collateralize extensively within
567 the cerebellar cortex with some axons crossing the midline. We also discover that cervical *Atoh1*-lineage
568 neurons make up the indirect spino-LRt and spino-olivary pathways while thoracolumbar *Atoh1*-lineage
569 neurons project mostly locally within the spinal cord. In contrast to CC neurons, cervical and
570 thoracolumbar *Atoh1*-lineage neurons make direct connections to MNs and these local connections likely
571 underlie the subtle motor defect seen when a silencing gene is expressed in these neurons. Altogether,
572 we find that the proprioceptive circuits within the spinal cord consist of long-range direct (CC) as well as
573 indirect and locally-projecting (cervical and thoracolumbar *Atoh1*-lineage) neurons that likely mediate
574 different aspects of proprioception.

575 *Diversification of proprioceptive information through CC neurons*

576 We find many unique anatomical features of CC neurons that lend insight into how proprioceptive
577 information through CC neurons is relayed. First, we find that a couple thousand CC neurons make up
578 43-47% of the direct DSCT and VSCT pathways from the AZ relaying hindlimb proprioceptive information.

579 Second, our work clarifies that CC neurons synapse primarily on GCs and do not collateralize significantly
580 within the spinal cord, medulla, or CN, which has been a matter of debate in the literature (Ekerot and
581 Oscarsson, 1976; Szabo et al., 1990; Jiang et al., 2015; Luo et al., 2018). The fact that CC neurons do
582 not collateralize to other parts of the brainstem or CN, as is seen for other MF terminal sources (Sillitoe
583 et al., 2012; Beitzel et al., 2017), suggests that they are not involved in the integration of inputs with other
584 ascending or descending proprioceptive-motor pathways except at the GC level. Lastly, we do find,
585 though, that within the cerebellar cortex, CC neurons extensively diversify their MF terminals between
586 lobules, within a lobule, and even crossing the cerebellum to the contralateral side. Our estimate of
587 approximately 72 MF terminals for 1 CC soma at a population level is similar to the reported 99
588 terminals/neuron for CC neurons from single axon reconstructions (Luo et al., 2018). Part of the reason
589 for this expansion of proprioceptive information could be for parallel processing across many domains of
590 the cerebellar cortex.

591 *Atoh1-lineage spino-LRt and spino-olivary neurons*

592 We initially hypothesized that *Atoh1*-lineage neurons made lamina V-SCT or dhSCT neurons
593 based on their anatomical location and developmental studies that reported *Atoh1*-lineage axons go to
594 the cerebellum (Matsushita and Hosoya, 1979; Bermingham et al., 2001; Sakai et al., 2012; Yuengert et
595 al., 2015). Instead, we found that cervical *Atoh1*-lineage neurons make mainly the indirect spino-LRt and
596 spino-olivary pathways. Thus, the cerebellar axonal projections seen during development either extend
597 to the cerebellum and retract during development or die. However, it is possible that *Atoh1*-lineage
598 neurons make a subset of direct spinocerebellar neurons that project to the posterior zone (PZ – lobules
599 VIII/IXa), which was not assessed in our study. Cervical *Atoh1*-lineage neurons could contribute to any
600 of three possible spino-LRt populations that function in posture (bilateral ventral reflex tract), reaching
601 (propriospinal), or grasping (ipsilateral forelimb tract)(Alstermark and Ekerot, 2013; Jiang et al., 2015).
602 We found that cervical *Atoh1*-lineage neurons appear to target the LRt ipsilaterally and as a population
603 can synapse on MNs as well, therefore, it seems likely that *Atoh1*-lineage neurons are at least
604 propriospinal spino-LRt neurons. For the spino-olivary pathway, we found cervical *Atoh1*-lineage neurons

505 targeted areas of the IO (dfDAO, DAO, cMAO[a], cMAO[b]) consistent with previously described tracing
506 studies and that retrograde tracing from the IO colocalizes with *Atoh1*-lineage neurons in laminae V-VIII
507 (Swenson and Castro, 1983a, b; Matsushita et al., 1992; Oldenbeuving et al., 1999; Flavell et al., 2014).
508 Overall, though, there are numerous other spino-LRt and spino-olivary neurons in the spinal cord
509 suggesting that there are additional sources that are not from the *Atoh1*-lineage (Azim et al., 2014; Pivetta
510 et al., 2014; Choi et al., 2020).

511 *Local projections of Atoh1-lineage neurons*

512 We find some interesting features of locally-projecting *Atoh1*-lineage neurons and compare and
513 contrast our findings with those of a previous study using an *Atoh1*-enhancer driving CRE recombinase
514 electroporated into mouse embryos (Kaneyama and Shirasaki, 2018). First, we find that thoracolumbar
515 *Atoh1*-lineage neurons project mostly locally, consistent with the findings by Kaneyama and Shiraskai,
516 who found that crossing dI1 axons are intersegmental with only a few traveling far from the soma. Second,
517 we found that *Atoh1*-lineage neurons in both the cervical and thoracolumbar areas of the mature spinal
518 cord make local circuit connections with MNs as previously described during embryogenesis and thus,
519 are a source of pre-motor neurons (Goetz et al., 2015). Kaneyama and Shiraskai found that dI1
520 commissural axons made synapses on axial MNs, while we found that *Atoh1*-lineage neurons as a
521 population can target the lateral motor column as well. Lastly, similar to our findings, Kaneyama and
522 Shiraskai also found that some dI1 commissural axons come from a fairly dorsolateral population, rather
523 than a medial population, and that these neurons in the lateral population appear to project both
524 contralaterally and ipsilaterally.

525 *Comparison of motor behaviors mediated by proprioceptive spinal pathways*

526 Loss of proprioceptive input in animal models leads to defects in limb coordination and lack of
527 adaptation to uneven surfaces (Abelew et al., 2000; Windhorst, 2007; Akay et al., 2014). Differences in
528 circuitry between CC (long-range) and caudal *Atoh1*-lineage neurons (indirect and local) suggests that
529 different aspects of proprioceptive-motor behaviors could be mediated by separable microcircuits. We
530 examined the function of CC and caudal *Atoh1*-lineage neurons by expressing a silencing gene,

531 tetanus toxin light chain, in these neurons. Motor function and motor learning were unimpaired when we
532 attempted to silence CC neurons (data not shown), possibly due to sparse expression of our silencing
533 allele, attenuated activity of the silencing allele, or redundancy or compensation of the proprioceptive-
534 motor system. In contrast, we found a slight motor defect in the accelerating rotarod when we silenced
535 caudal *Atoh1*-lineage neurons, consistent with a potential defect in reflexive behavior or postural
536 adjustments that would occur in local circuits.

537 To assess the function of cervical *Atoh1*-lineage neurons that contribute to the spino-LRt tract,
538 we assessed the behavior of the silenced caudal *Atoh1*-lineage mice in a pellet reaching task (Azim et
539 al., 2014; Becker et al., 2020). We analyzed the reach in five control mice and seven silenced caudal
540 *Atoh1*-lineage littermates, but we did not see any significant differences in pellet reach trajectories due
541 to the low sample size and potentially attenuated function of the TeTx allele (data not shown).

542 Cervical *Atoh1*-lineage neurons also contribute to the spino-olivary tract. We are not aware of any
543 studies that have manipulated the activity of spino-olivary neurons. However, mice that had glutamatergic
544 signaling in IO neurons knocked out had dystonia-like features, such as twisting, stiff limbs, and tremor,
545 and were unable to perform on the accelerating rotarod test (White and Sillitoe, 2017). We saw no overt
546 twisting, stiff limbs, or tremor in the genetically silenced caudal *Atoh1*-lineage mice, however, these mice
547 did have a defect in the accelerating rotarod and similarly, mice that had *Atoh1* knocked out caudal to
548 the lower medulla were completely unable to perform the rotarod test (Yuengert et al., 2015), suggesting
549 that the spino-olivary system is important for updating motor outcomes. Altogether, caudal *Atoh1*-lineage
550 neurons are heterogeneous comprising parts of the spino-LRt and spino-olivary tracts as well as
551 projecting locally within the spinal cord. Future experiments uncoupling the function of these different
552 components using more robust ablation or acute silencing strategies will lend further insight into the
553 function of discrete proprioceptive circuits.

554 *Future directions*

555 Our work and others suggest that the spinocerebellar and spino-LRt systems come from several
556 developmental progenitor domains and that any given developmental progenitor domain (*Atoh1*, for

example) contributes to several neuronal types (minimally, spino-LRt and spino-olivary tracts, as well as local spinal neurons). Comparing and contrasting features of neurons with similar anatomical connectivity but generated from different progenitor domains may lend insights into the varied functions mediated by seemingly similar anatomical classes. Conversely, separating out different pathways, such as the spino-LRt and spino-olivary tracts that are generated from a single progenitor domain (*Atoh1*) will be important for determining the separate functions of these pathways.

We found that direct CC neurons do not send significant axon collaterals to the LRt or IO and that information to the LRt and IO are in part coming from *Atoh1*-lineage neurons. Therefore, the MF and CF input coming from the spinal cord into the cerebellar cortex comes from different information streams and are not simply collateral copies of the direct CC pathway. Future work focused on how the direct and indirect information streams from the spinal cord either converge or diverge within the cerebellar cortex and the timing with which this information comes in from the two different information streams will be particularly interesting.

References:

Abelew TA, Miller MD, Cope TC, Nichols TR (2000) Local loss of proprioception results in disruption of interjoint coordination during locomotion in the cat. J Neurophysiol 84:2709-2714.

Akay T, Tourtellotte WG, Arber S, Jessell TM (2014) Degradation of mouse locomotor pattern in the absence of proprioceptive sensory feedback. Proc Natl Acad Sci U S A 111:16877-16882.

Albus JS (1971) Mathematical biosciences. In, p volumes. New York,: Elsevier.

Alstermark B, Ekerot CF (2013) The lateral reticular nucleus: a precerebellar centre providing the cerebellum with overview and integration of motor functions at systems level. A new hypothesis. J Physiol 591:5453-5458.

Apps R, Hawkes R (2009) Cerebellar cortical organization: a one-map hypothesis. Nat Rev Neurosci 10:670-681.

Arsenio Nunes ML, Sotelo C (1985) Development of the spinocerebellar system in the postnatal rat. J Comp Neurol 237:291-306.

Avraham O, Hadas Y, Vald L, Zisman S, Schejter A, Visel A, Klar A (2009) Transcriptional control of axonal guidance and sorting in dorsal interneurons by the Lim-HD proteins Lhx9 and Lhx1. Neural Dev 4:21.

Azim E, Jiang J, Alstermark B, Jessell TM (2014) Skilled reaching relies on a V2a propriospinal internal copy circuit. Nature 508:357-363.

Baek M, Menon V, Jessell TM, Hantman AW, Dasen JS (2019) Molecular Logic of Spinocerebellar Tract Neuron Diversity and Connectivity. Cell Rep 27:2620-2635 e2624.

Becker MI, Calame DJ, Wrobel J, Person AL (2020) Online control of reach accuracy in mice. J Neurophysiol 124:1637-1655.

Beitzel CS, Houck BD, Lewis SM, Person AL (2017) Rubrocerebellar Feedback Loop Isolates the Interposed Nucleus as an Independent Processor of Corollary Discharge Information in Mice. J Neurosci 37:10085-10096.

696 Berkley KJ, Worden IG (1978) [Projections to the inferior olive of the cat. I. Comparisons of input from
697 the dorsal column nuclei, the lateral cervical nucleus, the spino-olivary pathways, the cerebral
698 cortex and the cerebellum]. J Comp Neurol 180:237-251.
699 Bermingham NA, Hassan BA, Wang VY, Fernandez M, Banfi S, Bellen HJ, Fritzsch B, Zoghbi HY
700 (2001) Proprioceptor pathway development is dependent on Math1. Neuron 30:411-422.
701 Bosco G, Poppele RE (2001) Proprioception from a spinocerebellar perspective. Physiol Rev 81:539-
702 568.
703 Bourane S, Grossmann KS, Britz O, Dalet A, Del Barrio MG, Stam FJ, Garcia-Campmany L, Koch S,
704 Goulding M (2015) Identification of a spinal circuit for light touch and fine motor control. Cell
705 160:503-515.
706 Cebrian C, Asai N, D'Agati V, Costantini F (2014) The number of fetal nephron progenitor cells limits
707 ureteric branching and adult nephron endowment. Cell Rep 7:127-137.
708 Choi S, Hachisuka J, Brett MA, Magee AR, Omori Y, Iqbal NU, Zhang D, DeLisle MM, Wolfson RL, Bai
709 L, Santiago C, Gong S, Goulding M, Heintz N, Koerber HR, Ross SE, Ginty DD (2020) Parallel
710 ascending spinal pathways for affective touch and pain. Nature 587:258-263.
711 Cummings JF, Petras JM (1977) The origin of spinocerebellar pathways. I. The nucleus cervicalis
712 centralis of the cranial cervical spinal cord. J Comp Neurol 173:655-692.
713 Eccles JC, Ito M, Szentágothai Jn (1967) The cerebellum as a neuronal machine. Berlin, New York
714 etc.: Springer-Verlag.
715 Edgley SA, Gallimore CM (1988) The morphology and projections of dorsal horn spinocerebellar tract
716 neurones in the cat. J Physiol 397:99-111.
717 Ekerot CJ, Oscarsson L (1976) The lateral reticular nucleus in the cat. V. Does collateral activation from
718 the dorsal spinocerebellar tract occur? Exp Brain Res 25:327-337.
719 Flavell CR, Cerminara NL, Apps R, Lumb BM (2014) Spino-olivary projections in the rat are
720 anatomically separate from postsynaptic dorsal column projections. J Comp Neurol 522:2179-
721 2190.

722 Gebre SA, Reeber SL, Sillitoe RV (2012) Parasagittal compartmentation of cerebellar mossy fibers as
723 revealed by the patterned expression of vesicular glutamate transporters VGLUT1 and
724 VGLUT2. Brain Struct Funct 217:165-180.
725 Gilmer JI, Person AL (2017) Morphological Constraints on Cerebellar Granule Cell Combinatorial
726 Diversity. J Neurosci 37:12153-12166.
727 Goetz C, Pivetta C, Arber S (2015) Distinct limb and trunk premotor circuits establish laterality in the
728 spinal cord. Neuron 85:131-144.
729 Gordon J, Ghilardi MF, Ghez C (1995) Impairments of reaching movements in patients without
730 proprioception. I. Spatial errors. J Neurophysiol 73:347-360.
731 Gowan K, Helms AW, Hunsaker TL, Collisson T, Ebert PJ, Odom R, Johnson JE (2001) Crossinhibitory
732 activities of Ngn1 and Math1 allow specification of distinct dorsal interneurons. Neuron 31:219-
733 232.
734 Gray EG (1961) The granule cells, mossy synapses and Purkinje spine synapses of the cerebellum:
735 light and electron microscope observations. J Anat 95:345-356.
736 Hantman AW, Jessell TM (2010) Clarke's column neurons as the focus of a corticospinal corollary
737 circuit. Nat Neurosci 13:1233-1239.
738 Houck BD, Person AL (2015) Cerebellar Premotor Output Neurons Collateralize to Innervate the
739 Cerebellar Cortex. J Comp Neurol 523:2254-2271.
740 Huang CC, Sugino K, Shima Y, Guo C, Bai S, Mensh BD, Nelson SB, Hantman AW (2013)
741 Convergence of pontine and proprioceptive streams onto multimodal cerebellar granule cells.
742 eLife 2:e00400.
743 Jakab RL, Hamori J (1988) Quantitative morphology and synaptology of cerebellar glomeruli in the rat.
744 Anat Embryol (Berl) 179:81-88.
745 Ji Z, Hawkes R (1994) Topography of Purkinje cell compartments and mossy fiber terminal fields in
746 lobules II and III of the rat cerebellar cortex: spinocerebellar and cuneocerebellar projections.
747 Neuroscience 61:935-954.

748 Jiang J, Azim E, Ekerot CF, Alstermark B (2015) Direct and indirect spino-cerebellar pathways: shared
749 ideas but different functions in motor control. Front Comput Neurosci 9:75.
750 Kaneyama T, Shirasaki R (2018) Post-crossing segment of dI1 commissural axons forms collateral
751 branches to motor neurons in the developing spinal cord. J Comp Neurol 526:1943-1961.
752 Kato S, Kobayashi K, Kobayashi K (2014) Improved transduction efficiency of a lentiviral vector for
753 neuron-specific retrograde gene transfer by optimizing the junction of fusion envelope
754 glycoprotein. J Neurosci Methods 227:151-158.
755 Kim JC, Cook MN, Carey MR, Shen C, Regehr WG, Dymecki SM (2009) Linking genetically defined
756 neurons to behavior through a broadly applicable silencing allele. Neuron 63:305-315.
757 Liang H, Bacskai T, Paxinos G (2015) Termination of vestibulospinal fibers arising from the spinal
758 vestibular nucleus in the mouse spinal cord. Neuroscience 294:206-214.
759 Llewellyn-Smith IJ, Martin CL, Fenwick NM, Dicarlo SE, Lujan HL, Schreihofer AM (2007) VGLUT1 and
760 VGLUT2 innervation in autonomic regions of intact and transected rat spinal cord. J Comp
761 Neurol 503:741-767.
762 Luo Y, Patel RP, Sarpong GA, Sasamura K, Sugihara I (2018) Single axonal morphology and
763 termination to cerebellar aldolase C stripes characterize distinct spinocerebellar projection
764 systems originating from the thoracic spinal cord in the mouse. J Comp Neurol 526:681-706.
765 Madisen L, Zwingman TA, Sunkin SM, Oh SW, Zariwala HA, Gu H, Ng LL, Palmiter RD, Hawrylycz MJ,
766 Jones AR, Lein ES, Zeng H (2010) A robust and high-throughput Cre reporting and
767 characterization system for the whole mouse brain. Nat Neurosci 13:133-140.
768 Madisen L et al. (2015) Transgenic mice for intersectional targeting of neural sensors and effectors with
769 high specificity and performance. Neuron 85:942-958.
770 Malet M, Vieytes CA, Lundgren KH, Seal RP, Tomasella E, Seroogy KB, Hokfelt T, Gebhart GF,
771 Brumovsky PR (2013) Transcript expression of vesicular glutamate transporters in lumbar
772 dorsal root ganglia and the spinal cord of mice - Effects of peripheral axotomy or hindpaw
773 inflammation. Neuroscience 248:95-111.

774 Manni E, Petrosini L (2004) A century of cerebellar somatotopy: a debated representation. Nat Rev
775 Neurosci 5:241-249.
776 Marr D (1969) A theory of cerebellar cortex. J Physiol 202:437-470.
777 Matsushita M, Ikeda M (1970) Spinal projections to the cerebellar nuclei in the cat. Exp Brain Res
778 10:501-511.
779 Matsushita M, Hosoya Y (1979) Cells of origin of the spinocerebellar tract in the rat, studied with the
780 method of retrograde transport of horseradish peroxidase. Brain Res 173:185-200.
781 Matsushita M, Gao X (1997) Projections from the thoracic cord to the cerebellar nuclei in the rat,
782 studied by anterograde axonal tracing. J Comp Neurol 386:409-421.
783 Matsushita M, Yaginuma H, Tanami T (1992) Somatotopic termination of the spino-olivary fibers in the
784 cat, studied with the wheat germ agglutinin-horseradish peroxidase technique. Exp Brain Res
785 89:397-407.
786 Mogensen H, Bengtsson F, Jorntell H (2017) No Medium-Term Spinocerebellar Input Plasticity in Deep
787 Cerebellar Nuclear Neurons In Vivo? Cerebellum 16:638-647.
788 Nanes BA (2015) Slide Set: Reproducible image analysis and batch processing with ImageJ.
789 Biotechniques 59:269-278.
790 Ogujiofor OW, Pop IV, Espinosa F, Durodoye RO, Viacheslavov ML, Jarvis R, Landy MA, Gurumurthy
791 CB, Lai HC (2021) An Atoh1 CRE Knock-In Mouse Labels Motor Neurons Involved in Fine
792 Motor Control. eNeuro 8.
793 Oldenbeuving AW, Eisenman LM, De Zeeuw CI, Ruigrok TJ (1999) Inferior olivary-induced expression
794 of Fos-like immunoreactivity in the cerebellar nuclei of wild-type and Lurcher mice. Eur J
795 Neurosci 11:3809-3822.
796 Oscarsson O (1965) Functional Organization of the Spino- and Cuneocerebellar Tracts. Physiol Rev
797 45:495-522.
798 Oscarsson O, Sjolund B (1977a) The ventral spine-olivocerebellar system in the cat. II. Termination
799 zones in the cerebellar posterior lobe. Exp Brain Res 28:487-503.

300 Oscarsson O, Sjolund B (1977b) The ventral spino-olivocerebellar system in the cat. I. Identification of
301 five paths and their termination in the cerebellar anterior lobe. Exp Brain Res 28:469-486.
302 Park YG et al. (2018) Protection of tissue physicochemical properties using polyfunctional crosslinkers.
303 Nat Biotechnol.
304 Paxinos G, Franklin KBJ (2007) The Mouse Brain in Stereotaxic Coordinates, Third Edition. San Diego:
305 Academic Press.
306 Pivetta C, Esposito MS, Sigrist M, Arber S (2014) Motor-circuit communication matrix from spinal cord
307 to brainstem neurons revealed by developmental origin. Cell 156:537-548.
308 Popova LB, Ragnarson B, Orlovsky GN, Grant G (1995) Responses of neurons in the central cervical
309 nucleus of the rat to proprioceptive and vestibular inputs. Archives italiennes de biologie 133:31-
310 45.
311 Quinones HI, Savage TK, Battiste J, Johnson JE (2010) Neurogenin 1 (Neurog1) expression in the
312 ventral neural tube is mediated by a distinct enhancer and preferentially marks ventral
313 interneuron lineages. Dev Biol.
314 Reeber SL, Gebre SA, Sillitoe RV (2011) Fluorescence mapping of afferent topography in three
315 dimensions. Brain Struct Funct 216:159-169.
316 Rodrigues DM, Li AY, Nair DG, Blennerhassett MG (2011) Glial cell line-derived neurotrophic factor is a
317 key neurotrophin in the postnatal enteric nervous system. Neurogastroenterol Motil 23:e44-56.
318 Rose MF, Ahmad KA, Thaller C, Zoghbi HY (2009) Excitatory neurons of the proprioceptive,
319 interoceptive, and arousal hindbrain networks share a developmental requirement for Math1.
320 Proc Natl Acad Sci U S A 106:22462-22467.
321 Sakai N, Insolera R, Sillitoe RV, Shi SH, Kaprielian Z (2012) Axon sorting within the spinal cord
322 marginal zone via Robo-mediated inhibition of N-cadherin controls spinocerebellar tract
323 formation. J Neurosci 32:15377-15387.

324 Schindelin J, Arganda-Carreras I, Frise E, Kaynig V, Longair M, Pietzsch T, Preibisch S, Rueden C,
325 Saalfeld S, Schmid B, Tinevez JY, White DJ, Hartenstein V, Eliceiri K, Tomancak P, Cardona A
326 (2012) Fiji: an open-source platform for biological-image analysis. Nat Methods 9:676-682.
327 Sengul G, Fu Y, Yu Y, Paxinos G (2015) Spinal cord projections to the cerebellum in the mouse. Brain
328 Struct Funct 220:2997-3009.
329 Shambes GM, Gibson JM, Welker W (1978) Fractured somatotopy in granule cell tactile areas of rat
330 cerebellar hemispheres revealed by micromapping. Brain Behav Evol 15:94-140.
331 Sherrington CS (1906) The Integrative Action of the Nervous System. New Haven, CT: Yale University
332 Press.
333 Sillitoe RV, Fu YH, Watson C (2012) The mouse nervous system. In, 1st Edition (Watson C, Paxinos G,
334 Puelles L, eds), pp pp.360-397. Amsterdam ; Boston: Elsevier Academic Press.
335 Soriano P (1999) Generalized lacZ expression with the ROSA26 Cre reporter strain. Nat Genetics
336 21:70-71.
337 Suzuki H, Hase A, Miyata Y, Arahata K, Akazawa C (1998) Prominent expression of glial cell line-
338 derived neurotrophic factor in human skeletal muscle. J Comp Neurol 402:303-312.
339 Swenson RS, Castro AJ (1983a) The afferent connections of the inferior olivary complex in rats. An
340 anterograde study using autoradiographic and axonal degeneration techniques. Neuroscience
341 8:259-275.
342 Swenson RS, Castro AJ (1983b) The afferent connections of the inferior olivary complex in rats: a study
343 using the retrograde transport of horseradish peroxidase. Am J Anat 166:329-341.
344 Szabo T, Libouban S, Denizot JP (1990) A well defined spinocerebellar system in the weakly electric
345 teleost fish Gnathonemus petersii. A tracing and immuno-histochemical study. Archives
346 italiennes de biologie 128:229-247.
347 Trupp M, Ryden M, Jornvall H, Funakoshi H, Timmusk T, Arenas E, Ibanez CF (1995) Peripheral
348 expression and biological activities of GDNF, a new neurotrophic factor for avian and
349 mammalian peripheral neurons. J Cell Biol 130:137-148.

350 Tuthill JC, Azim E (2018) Proprioception. Curr Biol 28:R194-R203.

351 Watson C, Paxinos G, Kayalioglu G (2009) The Spinal Cord: A Christopher and Dana Reeve
352 Foundation Text and Atlas. New York: Academic Press.

353 White JJ, Sillitoe RV (2017) Genetic silencing of olivocerebellar synapses causes dystonia-like
354 behaviour in mice. Nat Commun 8:14912.

355 Wiksten B (1987) Further studies on the fiber connections of the central cervical nucleus in the cat. Exp
356 Brain Res 67:284-290.

357 Wilson SI, Shafer B, Lee KJ, Dodd J (2008) A molecular program for contralateral trajectory: Rig-1
358 control by LIM homeodomain transcription factors. Neuron 59:413-424.

359 Windhorst U (2007) Muscle proprioceptive feedback and spinal networks. Brain Res Bull 73:155-202.

360 Yang H, Xie X, Deng M, Chen X, Gan L (2010) Generation and characterization of Atoh1-Cre knock-in
361 mouse line. Genesis 48:407-413.

362 Yuengert R, Hori K, Kibodeaux EE, McClellan JX, Morales JE, Huang TW, Neul JL, Lai HC (2015)
363 Origin of a Non-Clarke's Column Division of the Dorsal Spinocerebellar Tract and the Role of
364 Caudal Proprioceptive Neurons in Motor Function. Cell Rep 13:1258-1271.

365

366

367 **Legends**

368 **Figure 1. Clarke's column (CC) is the major direct spinocerebellar pathway in mice.** (A) Lineage
369 tracing of *Neurog1*-expressing progenitors (*Neurog1BAC-Cre* crossed to *R26*$^{LSL\text{-}LacZ}$) in the neural tube
370 identifies large CC neurons in the thoracic spinal cord (box in X-gal stain). β-Gal expressing cells (green)
371 colocalize with the CC marker, *Vglut1* mRNA (magenta, arrows). *Atoh1*-lineage neurons (*Atoh1*^{Tom})
372 reside lateral and ventral to CC. (B) CC is marked by expression of *Gdnf* and *Vglut1* mRNA. (C) *Gdnf*
373 and *Vglut1* mRNA colocalize in CC neurons at P10 by RNAscope (arrowheads). (D) CC neurons
374 retrogradely labeled with fluorogold (FG) colocalize with *Vglut1* mRNA (FG^{+}*Vglut1*$^{+}$, arrowheads). A
375 subset of CC neurons are labeled with *Gdnf*^{Tom} (FG^{+}TOM^{+}*Vglut1*$^{+}$, arrows). (E) CC neurons marked by
376 *Gdnf*^{Tom} express both *Vglut1* and *Vglut2* mRNA (arrowheads). (F-I) Comparison of mossy fiber (MF)
377 terminals in the cerebellum of CC and caudal *Atoh1*-lineage neurons. Diagram of CC and caudal *Atoh1*-
378 lineage neurons labeled with tdTomato (TOM)(F, G). MF terminals in the cerebellum of CC neurons are
379 VGLUT1^{+} (VG1) and VGLUT2^{+} (VG2) (F', arrows). MF terminals of caudal *Atoh1*-lineage neurons are
380 VG2^{+} (G', arrows), but VG1^{-} (G', arrowheads). Fewer MF terminals are seen in the cerebellum from
381 caudal *Atoh1*-lineage neurons (G'') than CC neurons (F''). Representative thoracic sections of CC and
382 caudal *Atoh1*-lineage neurons (F''', G'''). Quantitation of MF terminals in the vermis of lobules I-V and
383 VIII/IX (H) and of the number of soma in the spinal cord (I) for CC and caudal *Atoh1*-lineage neurons. (J-
384 P) Comparison of spinocerebellar neurons retrogradely labeled with FG in mice with CC (*Gdnf*^{Tom}) or
385 *Atoh1*-lineage (*Atoh1*^{Tom}) neurons labeled with tdTomato (TOM). Diagram of FG cerebellar injections into
386 the anterior zone (AZ, lobules I-V) of either *Gdnf*^{Tom} or *Atoh1*^{Tom} mice to retrogradely label direct
387 spinocerebellar projections (J). FG injection in the cerebellum (K, N, green) retrogradely labels central
388 cervical (CeCv) cells in the cervical spinal cord (K', N', upper panels), CC in the thoracic spinal cord (K',
389 N', middle panels), and neurons in other areas of the spinal cord (K', N', lower panels). Retrogradely
390 labeled CC neurons (green) colocalizes with the genetic label for CC (*Gdnf*^{Tom})(K', middle panel,
391 FG^{+}TOM^{+}, arrows), but only occasionally colocalizes with *Atoh1*-lineage (*Atoh1*^{Tom}) neurons in CeCv or
392 CC (N', arrows). Quantitation of the total number of FG^{+} cells (L, O) and percentage of total FG^{+} cells (M,

393 P) in a given region of the spinal cord (light orange or light blue) with the total number or percentage of
394 FG$^+$TOM$^+$ cells superimposed (dark orange or dark blue) for CC and caudal *Atoh1*-lineage neurons is
395 shown. Spinal cords were divided into cervical (C), thoracic (T), and lumbar (L) areas. The CeCv and CC
396 areas are delineated separately with all other cells categorized based on their C, T, or L location and
397 whether they were dorsal or ventral to the central canal. Spinocerebellar cells dorsal or ventral to the
398 central canal are generally not labeled by *Gdnf^{Tom}* or *Atoh1^{Tom}* (L, M, O, P). Abbrev: P, postnatal. Scale
399 bars: 1 mm (K, N), 100 μm (A-E, F''-F''', G''-G''', K', N'), 10 μm (F',G'). Results in graphs presented as
900 mean ± SEM.

901 **Figure 2. CC mossy fibers terminate ipsilaterally and contralaterally in the cerebellar vermis.** (A-
902 C) Coronal sections from *Gdnf^{Tom}* mice reveal CC mossy fiber (MF) terminals (TOM$^+$) in lobules II-V, VIII,
903 IXa, and the copula (C, Cop, arrows). Parasagittal stripes (1, 2, 3) in lobule III are apparent. (D-E) Some
904 CC axons (TOM$^+$) cross the midline (D, arrow, cryosection, and E, arrows, cleared sample, 200 μm
905 maximum intensity projection (MIP)). (F) Diagram of dual CTB-488 and CTB-647 injections in *Gdnf^{Tom}*
906 mice. (G) Coronal section showing the injection site of CTB-488 and CTB-647. (H) CC neurons are co-
907 labeled with the fluorescent CTB injected on the ipsilateral side as well as the fluorescent CTB injected
908 on the contralateral side (CTB-488$^+$CTB-647$^+$, arrows and arrowheads,). Some cells also colocalize with
909 the *Gdnf^{Tom}* genetic label for CC (TOM$^+$CTB-488$^+$CTB-647$^+$, arrows) and some do not (TOM$^-$CTB-
910 488$^+$CTB-647$^+$, arrowheads). (I) Quantitation of the percentage of ipsilaterally or contralaterally labeled
911 CTB$^+$ cells out of all CTB$^+$ cells labeled in the spinal cord with a particular CTB fluorophore (mean ± SEM).
912 Abbrev: Med, Medial; Int, Interpositus; Lat, Lateral. Scale bars: 1 mm (A, B, C, G), 100 μm (D, E, H).

913 **Figure 3. CC neurons do not collateralize to the medulla or cerebellar nuclei (CN), but arborize**
914 **extensively in the cerebellar cortex.** (A-D'') Almost no CC *Gdnf^{Tom}* axons enter or are near the CN
915 (arrowheads, Med, Int, Lat)(A, B, C, and D are successive sections 160 μm apart). Areas of TOM$^+$ signal
916 near CN do not colocalize with presynaptic markers VG1 (A', D') or VG2 (A'', D'') indicating these are
917 axons of passage and not presynaptic terminals. (E) CC axons (TOM$^+$) avoid the CN in another *Gdnf^{Tom}*
918 mouse whose cerebellum was cleared (100 μm MIP). (F) CC axons (TOM$^+$) avoid the CN (40 μm

919 cryosection) in another example *Gdnf*^{Tom} mouse. Images are from two female (A-E) and one male (F)
920 mice (n=3). (G-H') Only a few axonal terminations are seen in the LRt (G-G', arrow) and none in nucleus
921 X (H-H')(verified in n=3 mice, representative sections shown). (I-K) Example images of 100 μm MIP from
922 a *Gdnf*^{Tom} cleared cerebellum. CC MF terminals (TOM^{+}) are seen in II-V, VIII, IXa, and Cop. (K)
923 Quantification of the MF/cell body ratio (n=3 mice, one *Gdnf*^{Tom} and two *Gdnf*^{CreER}*; Cdx2::FLPo; Ai65*
924 mice). Overall the whole cerebellum (Cb) has an estimated 71.9 MF terminals per CC cell body in the
925 spinal cord (orange bar, mean ± SEM). Most MF terminals from CC cells terminate in I-III, IV/V, VIII/IXa,
926 and Cop (light orange bars). Abbrev: Med, Medial; Int, Interpositus; Lat, Lateral. Lateral reticular nucleus,
927 LRt; X, Nucleus X; icp, inferior cerebellar peduncle; Sp5, spinal trigeminal tract. Scale bars: 1 mm (G, H,
928 I, I', J), 100 μm (A-F, G', H', J inset), 10 μm (A'-A'', D'-D'').

929 **Figure 4. Thoracolumbar CC MFs send diverse projections to multiple lobules.** (A-B') Spinal cord
930 injections of AAV9-Syn-DIO-EGFP at lower thoracic levels into *Gdnf*^{Tom} mice labels CC neurons on both
931 sides of the spinal cord (B', GFP^{+}TOM^{+} (arrows), GFP^{+} only (arrowheads)). (C-F) Examples of individual
932 MF axons and terminals from three mice: a cleared female mouse sample (C, 76 μm maximum intensity
933 projection (MIP)), one female mouse (D, 40 μm cryosection), and one male mouse (E, F, 40 μm
934 cryosection). Axons appear to have branching points (black arrowheads) and regularly spaced MF
935 terminals (white arrowheads)(C-D). MF terminals from an individual axon are spaced 50-80 μm apart (E-
936 F). (G-L''') Thoracolumbar injections whose MF terminations were analyzed in coronal sections.
937 Distribution of GFP^{+} cells in the spinal cord on left (orange) and right (light orange) sides (G, I, K, M, O,
938 Q). Schematics of coronal cerebellar sections of the spinal cord injections (G, I, K) indicating the location
939 of CC MF terminations (H-H''', J-J''', L-L''', TOM^{+}, red areas, respectively). Schematics of sagittal
940 cerebellar sections of the spinal cord injections (M, O, Q) indicating the location of CC MF terminations
941 (N, P, R, red areas, respectively). The subset of CC MF terminations that are from the lower thoracic-
942 lumbar region (GFP^{+}, green, and GFP^{+}TOM^{+}, yellow) are spread over multiple lobules (II-V, VIII). Certain
943 CC MF termination regions do not have thoracolumbar CC neuronal projections (red areas, arrowheads
944 with an absence of any GFP^{+} terminations). (S, T) Examples of CC MF terminations (GFP^{+}TOM^{+}, arrows,

945 and GFP^{+}-only arrowheads) in lobules III and VIII from 13-15 μm maximum intensity projections (MIP).
946 Scale bars: 100 μm (B, B', C, D, S, T); 10 μm (E, F).

947 **Figure 5. Spinal cord *Atoh1*-lineage neurons make spino-LRt and spino-olivary pathways.** (A)
948 Schematic of FG injections into the AZ of mice to identify LRt and IO neurons in the medulla. Axons of
949 caudal *Atoh1*-lineage neurons are genetically labeled (*Atoh1^{Cre}; Cdx2::FLPo; Ai65* mice). (B) FG injected
950 into lobules I-V. (C) Sparse cell bodies in the SpVe are detected in *Atoh1^{Cre}; Cdx2::FLPo; Ai65* mice. (D-
951 D'') TOM^{+} terminals seen in the lateral parabrachial (LPB) nucleus (D) are VG2^{+} (D'', arrows). (E-H'') A
952 high density of caudal *Atoh1*-lineage axons from the spinal cord are found in the LRt as well as areas of
953 the IO (dfDAO, DAO, cMAO^{a}, cMAO^{b}). (I-J) Caudal *Atoh1*-lineage axon terminals (TOM^{+}, magenta)
954 expressing the presynaptic VG2 marker (cyan) are closely apposed to retrogradely labeled FG^{+} cells in
955 the LRt (I) and IO (J)(arrows). Axonal terminations in the LRt and IO were verified in n=4 mice.
956 Representative sections shown in E-H''. Abbrev: ECu, external cuneate nucleus; IO, inferior olive;
957 cMAO^{a}, subnucleus a of caudal medial accessory olive; cMAO^{b}, subnucleus b of caudal medial accessory
958 olive; cMAO^{c}, subnucleus c of caudal medial accessory olive; MAO, medial accessory olive; DAO, dorsal
959 accessory olive; dfDAO, dorsal fold of the DAO; PO, principal olive; IRt, intermediate reticular nucleus;
960 LRt, lateral reticular nucleus; SpVe, spinal vestibular nucleus. Scale bars: 1 mm (B, D), 100 μm (C, D',
961 E-H''), 10 μm (D'', I, J).

962 **Figure 6. Cervical spinal cord *Atoh1*-lineage neurons project to the LRt and IO.** (A) Schematic of
963 FG injections into the right LRt and IO of *Atoh1^{Tom}* mice. (B-G) Retrogradely labeled *Atoh1*-lineage
964 neurons reside mainly in the cervical to upper thoracic levels. Four injections targeting the LRt and IO in
965 the medulla are shown (B, C, E, F – upper panels). The spinal cords of these four injections have dual
966 labeled cells (FG^{+}TOM^{+}) mainly in the cervical to upper thoracic regions (light purple - left side, light blue
967 - right side) with many other FG^{+} only cells elsewhere in the spinal cord (dark purple – left side, dark blue
968 - right side). Representative spinal cord sections of the injection in C is shown in D-D' and the injection
969 in F is shown in G-G''. *Atoh1*-lineage neurons in both the medial (G'') and lateral (D' and G') clusters are
970 retrogradely labeled with FG (arrowheads). (H) Schematic of dual recombinase anterograde tracing.

971 Lenti^{FugE}-Cre was injected into the right cervical spinal cord of *Atoh1*$^{P2A\text{-}FLPo}$; *Ai65* mice. (I-O'') Anterograde
972 tracing of *Atoh1*-lineage neurons finds axons in the LRt and IO. Injection of the right spinal cord (I) where
973 mostly neurons on the right side are labeled (J) has axonal projections to the right LRt, which express
974 the presynaptic marker VG2 (K-K', arrowheads). Injection of the right spinal cord (L) where *Atoh1*-lineage
975 neurons on both the left and right are labeled (M) has axonal projections to both the right LRt and IO,
976 specifically the cMAOb (N, O). The *Atoh1*-lineage axonal terminals (TOM$^+$) express the presynaptic
977 marker VG2 (white arrowheads) and are closely apposed to postsynaptic PSD95$^+$ punta (grey
978 arrowheads)(N', O', O''). (P) Schematic of inputs and local outputs of cervical *Atoh1*-lineage neurons. (Q-
979 Q') Synaptic terminals of proprioceptive afferents (VG1$^+$PV$^+$, white arrowheads) are closely apposed to
980 TOM$^+$ signal near medial and lateral *Atoh1*-lineage neurons. (R-R') Axons of cervical *Atoh1*-lineage
981 neurons synapse on motor neurons (VG2$^+$TOM$^+$ puncta closely apposed to PSD95$^+$ puncta on CHAT$^+$
982 motor neurons, white and grey arrowheads). CHAT$^+$ neurons in R-R' were imaged from the area of the
983 spinal cord indicated in L. Abbrev: nd, not determined. Scale bars: 100 μm (B, C, D-D', E, F, G-G'', I, K,
984 L, O, Q, Q'), 10 μm (K', N', O'-O'', Q-Q' high magnification, R-R' high magnification).

985 **Figure 7. Thoracolumbar *Atoh1*-lineage neurons project locally within the spinal cord.** (A) Diagram
986 of rostral to caudal sections of the spinal cord (LF (left-dark blue, right-blue); grey matter and VF (left-
987 purple, right-light blue)). Lenti^{FugE}-Cre was injected into *Atoh1*$^{P2A\text{-}FLPo}$*;Ai65* mice, such that *Atoh1*-lineage
988 neurons in the right thoracolumbar spinal cord were labeled. (B) Quantitation of the total estimated
989 number of infected cells (TOM$^+$) on the left and right sides. The virus appears to be taken up by axons of
990 passage that project from the contralateral side (see C). (C) Representative sections of the spinal cord
991 from a Lenti^{FugE}-Cre-injected *Atoh1*$^{P2A\text{-}FLPo}$*;Ai65* mouse. Cell bodies on the right side of the spinal cord
992 and axons in the right (Rt) LF (blue arrowhead) are labeled. Axons in the Rt VF (light blue arrowhead)
993 appear to be axons from cell bodies that are located on the contralateral side of the spinal cord (purple
994 arrows). Some axons in the left LF (dark blue arrowhead) are also seen. (D) L1-3 is the site of peak
995 infection (number of TOM$^+$ cell bodies labeled per section) and the number of cell bodies labeled tapers
996 off both rostrally and caudally further away from the injection site. (E) Very few axons on the right side

997 (blue (LF) and light blue (VF)) are detected in rostral sections (C6-8) compared to the site of injection L1-
998 3. (F-H') Distribution of infected cells in T11-13, L1-3, and L4-6 regions of the spinal cord (F, G, H, arrows
999 indicate injection on right side). Quantitation of the soma area size of infected medial (M), lateral (L), and
000 ventral (V) *Atoh1*-lineage neurons on the left and right sides of the spinal cord (F', G', H'). Inset in F
001 shows two cell bodies labeled on the left side contralateral to the injection that have projections extending
002 dorsolaterally and medioventrally (arrows). (I-I'') Some of the sparsely labeled thoracolumbar *Atoh1*-
003 lineage neurons have presynaptic terminals near (TOM^+VG2^+, arrowheads) or closely apposed (F'',
004 TOM^+VG2^+, arrowhead) to motor neurons ($CHAT^+$)(detected in n=4 samples, representative image
005 shown). See Materials and Methods and Results for details of quantitation for B, D, E, F', G', H'. Abbrev:
006 LF, lateral funiculus; VF, ventral funiculus. Scale bars: 100 μm (C, I), 10 μm (I', I''). Results in graphs
007 presented as mean ± SEM.

008 **Figure 8. Silencing of caudal *Atoh1*-lineage neurons leads to a subtle motor phenotype.** (A)
009 Schematic of dual recombinase strategy to silence caudal *Atoh1*-lineage neurons. (B) Mice heterozygous
010 for the TeTx allele in caudal *Atoh1*-lineage neurons are significantly impaired in the rotarod assay (two-
011 way ANOVA, $F(1,448) = 5.025$, $p=0.0255$ for genotype, Control: n=36 (20F:16M), Het: n=22 (10F:12M)).
012 (C-C') Upper cervical areas of the spinal cord in *Atoh1*^{Cre}*;Cdx2::FLPo;TeTx* mice only have *Atoh1*^{Cre}
013 expressed and thus, are $mCherry^+$ (C). Lumbar areas of the spinal cord that have both *Atoh1*^{Cre} and
014 *Cdx2::FLPo* expressed have lost the mCherry signal (C'). In both panels (C-C'), mCherry signal was
015 amplified using a dsRed antibody. Scale bars: 100 μm (C-C').

016 **Figure 9. Long-range direct and local indirect proprioceptive pathways.** (A) *Neurog1*-lineage
017 neurons of the developing neural tube generate CC neurons that project directly from the spinal cord to
018 the cerebellum while *Atoh1*-lineage neurons form mostly indirect spinocerebellar and local spinal
019 projections. (B) Schematic of major anatomical findings. CC neurons (orange) project ipsilaterally mainly
020 from the thoracic spinal cord directly to the cerebellum. Some CC axons cross the midline (dotted
021 orange). Cervical *Atoh1*-lineage neurons project mainly to the IO and LRt in the medulla (dark and light
022 blue). The LRt neurons then project either ipsilaterally or contralaterally to terminate in the cerebellar

023 cortex as MFs. The neurons in the IO then project contralaterally as well to synapse as climbing fiber
024 (CF) axons onto Purkinje cells (PCs) in the cerebellar cortex. Thoracolumbar *Atoh1*-lineage neurons
025 project mostly within the spinal cord (dark blue, horizontal arrows), although a few project to more rostral
026 regions within the medulla and cerebellum (dotted blue arrows). (C-D) Illustrations of long-range direct
027 and local indirect spinocerebellar pathways. CC neurons project rostrally in the ipsilateral funiculus where
028 they branch extensively in the cerebellum, avoiding the medulla and cerebellar nuclei (Med, Int, Lat) to
029 terminate in vermis I-V, VIII, IXa, and Cop (C). Some CC axons cross the midline within the cerebellum.
030 *Atoh1*-lineage neurons are heterogeneous with diverse projections. Cervical *Atoh1*-lineage neurons in
031 the spinal cord project both ipsilaterally and contralaterally to target mainly the LRt and IO in the hindbrain
032 (D). While we found that some of the *Atoh1*-lineage spino-LRt axons project ipsilaterally, whether some
033 spino-LRt projections come from the contralateral side was not determined in this study (question mark
034 along axons). The spino-IO tract is likely contralateral based on previous literature. *Atoh1*-lineage
035 neurons in the thoracolumbar area project mostly locally within the spinal cord. A few of the axons from
036 thoracolumbar *Atoh1*-lineage neurons may project to the medulla or cerebellar cortex (dotted blue).
037 Presynaptic terminals from *Atoh1*-lineage neurons are found on motor neurons (MN) in both the cervical
038 and thoracolumbar spinal cord. Abbrev: IRt, intermediate reticular nucleus; LRt, lateral reticular nucleus;
039 IO, inferior olive.

040 **Multimedia**

041 **Movie 1. *Gdnf^{Tom}* cleared spinal cord.** CC cell bodies line the thoracic midline with axons projecting to
042 the lateral funiculus (LF) and then turning rostrally. The *Gdnf^{Tom}* mouse line also labels smooth muscle
043 cells lining blood vessels within the spinal cord and along the meninges. TOM^{+} cells along the central
044 canal are also labeled.

045 **Movie 2. *Gdnf^{CreER}; Cdx2::FLPo; Ai65* cleared hindbrain.** CC axons terminate as mossy fibers (MF) in
046 the vermis of lobules I-V, VIII, IXa, and copula (cop). Axons from the spinal cord project directly to the
047 cerebellar cortex avoiding the medulla and cerebellar nuclei.

048 **Movie 3. *Atoh1^{Cre}; Cdx2::FLPo; Ai65* cleared spinal cord.** *Atoh1*-lineage neurons in the spinal cord
049 cluster into medial (M), lateral (L), and ventral (V) populations whose axons travel in the lateral and ventral
050 funiculi (LF and VF). tdTomato is misexpressed in sensory neurons.

051 **Movie 4. *Atoh1^{Cre}; Cdx2::FLPo; Ai65* cleared brain.** The most prominent axonal projections in *Atoh1^{Cre};*
052 *Cdx2::FLPo; Ai65* mice are to the lateral reticular nucleus (LRt) and inferior olive (IO). Although MF
053 projections are seen in cryosections, they are not obvious in the cleared spinal cord. There is diffuse
054 tdTomato fluorescence in the thalamus and cortex. The misexpression of tdTomato in sensory neurons
055 seen in the spinal cord is seen as projections to the cuneate (Cu), gracile (Gr), and external cuneate
056 nucleus (ECu).

057 **Movie 5**. **Three-dimensional projection of cells in the LRt of *Atoh1^{Cre}; Cdx2::FLPo; Ai65* mice.**
058 Cropped cell in Fig. 5I is taken from this z-stack of 0.5 μm optical slices with 0.25 μm step. Dense
059 terminations are seen in the LRt. FG (yellow), *Atoh1^{Cre}; Cdx2::FLPo; Ai65* axons (TOM^{+}, magenta), VG2
060 (cyan).

061 **Movie 6**. **Three-dimensional projection of cells in the IO of *Atoh1^{Cre}; Cdx2::FLPo; Ai65* mice.**
062 Cropped cell in Fig. 5J is taken from this z-stack of 0.5 μm optical slices with 0.25 μm step. Dense
063 terminations are seen in the IO. FG (yellow), *Atoh1^{Cre}; Cdx2::FLPo; Ai65* axons (TOM^{+}, magenta), VG2
064 (cyan).

065

Fig. 1

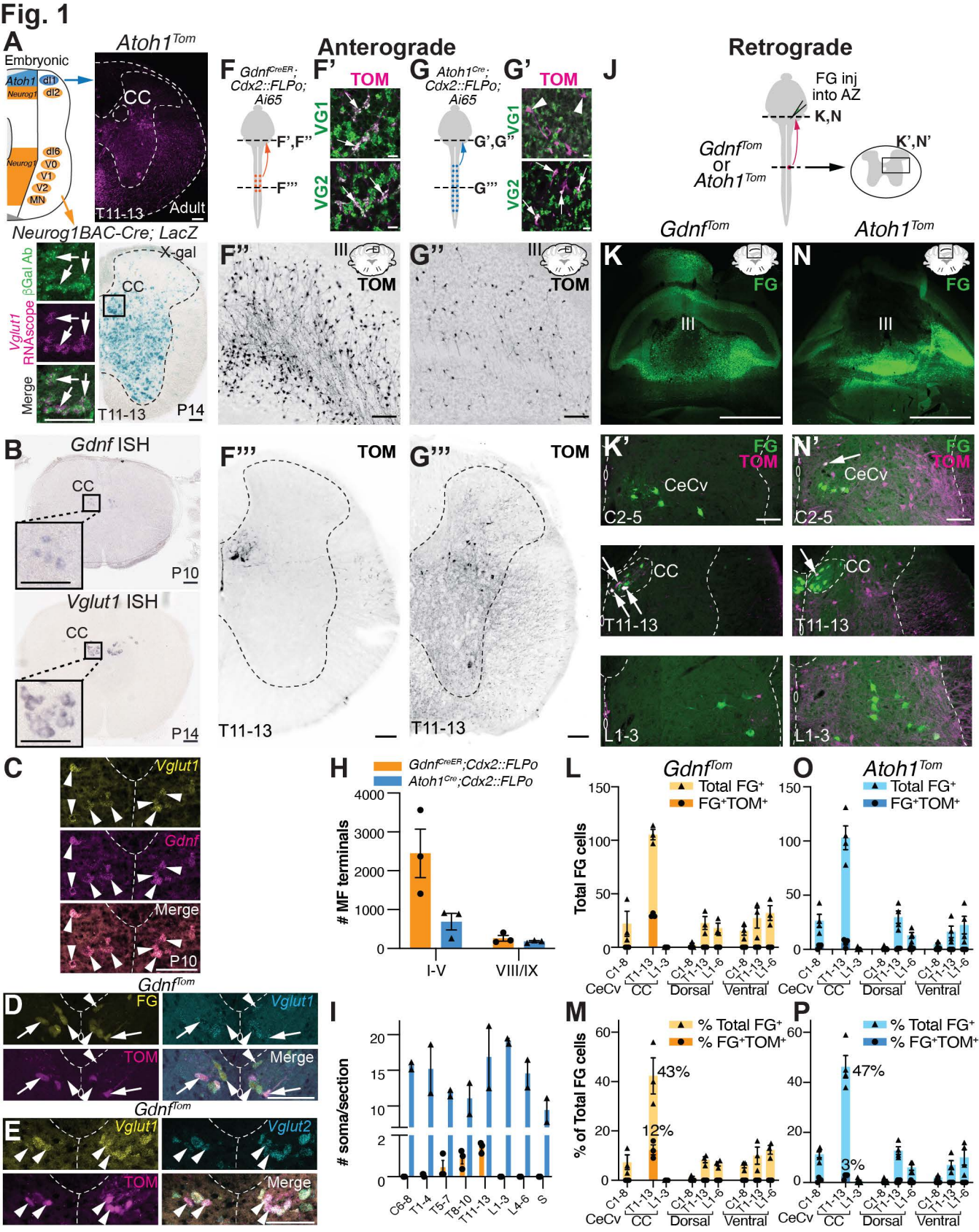
A
Atoh1Tom
Embryonic
Atoh1
Neurog1
dI1
dI2
dI6
V0
V1
V2
MN
CC
T11-13
Adult
Neurog1BAC-Cre; LacZ
βGal Ab
Vglut1 RNAscope
Merge
X-gal
P14
B
Gdnf ISH
P10
Vglut1 ISH
P14
C
Vglut1
Gdnf
Merge
P10
D
GdnfTom
FG
Vglut1
TOM
Merge
E
GdnfTom
Vglut1
Vglut2
TOM
Merge
Anterograde
F GdnfCreER; Cdx2::FLPo; Ai65
F'
TOM
VG1
VG2
F',F''
F'''
G Atoh1Cre; Cdx2::FLPo; Ai65
G'
G',G''
G'''
F''
G''
III
F'''
G'''
T11-13
Retrograde
J
FG inj into AZ
K,N
K',N'
GdnfTom or Atoh1Tom
K
N
FG
K'
N'
CeCv
C2-5
CC
L1-3
H
GdnfCreER;Cdx2::FLPo
Atoh1Cre;Cdx2::FLPo
MF terminals
I-V
VIII/IX
I
soma/section
C6-8
T1-4
T5-7
T8-10
T11-13
L1-3
L4-6
S
L
GdnfTom
Total FG+
FG+TOM+
Total FG cells
C1-8
T1-13
L1-3
L1-6
CeCv
CC
Dorsal
Ventral
M
% Total FG+
% FG+TOM+
% of Total FG cells
43%
12%
O
Atoh1Tom
P
47%
3%

Fig. 2

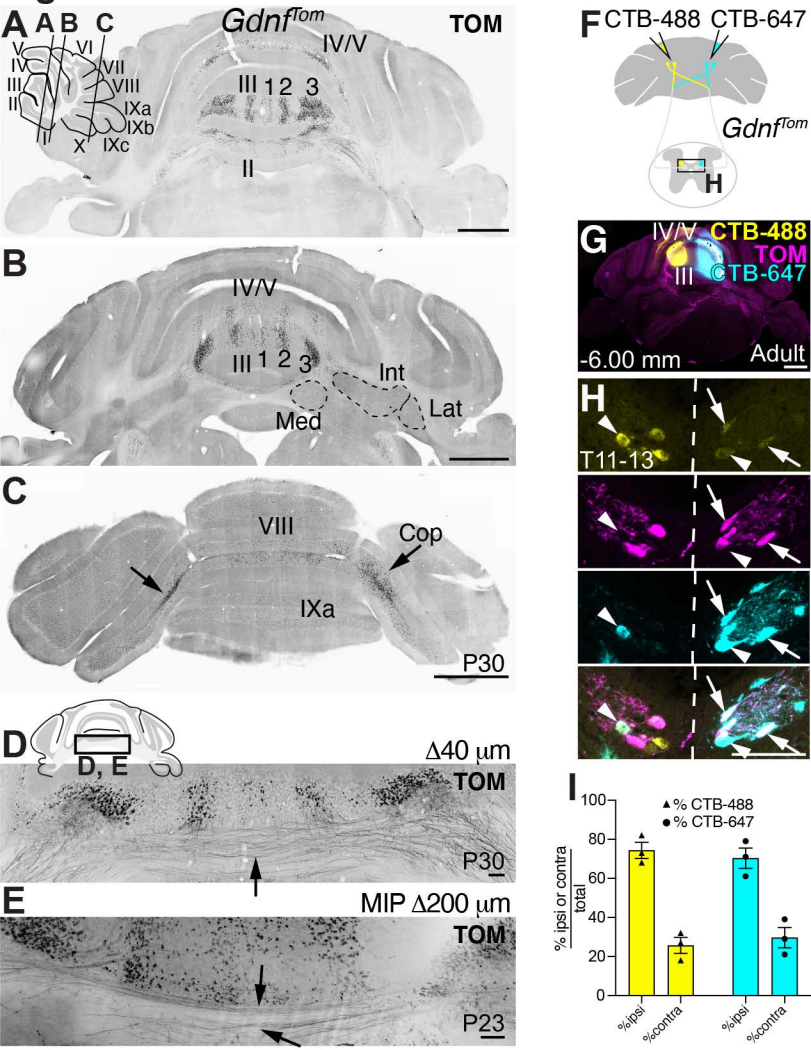
A
A B C
V
VI
IV
VII
III
VIII
IXa
II
IXb
I
X
IXc
Gdnf^Tom
TOM
IV/V
III 1 2 3
II
B
IV/V
III 1 2 3
Int
Med
Lat
C
VIII
Cop
IXa
P30
D
D, E
Δ40 μm
TOM
P30
E
MIP Δ200 μm
TOM
P23
F
CTB-488 CTB-647
Gdnf^Tom
H
G
IV/V
CTB-488
TOM
III
CTB-647
-6.00 mm
Adult
H
T11-13
I
% CTB-488
% CTB-647
% ipsi or contra / total
100
80
60
40
20
0
%ipsi
%contra
%ipsi
%contra

Fig. 3

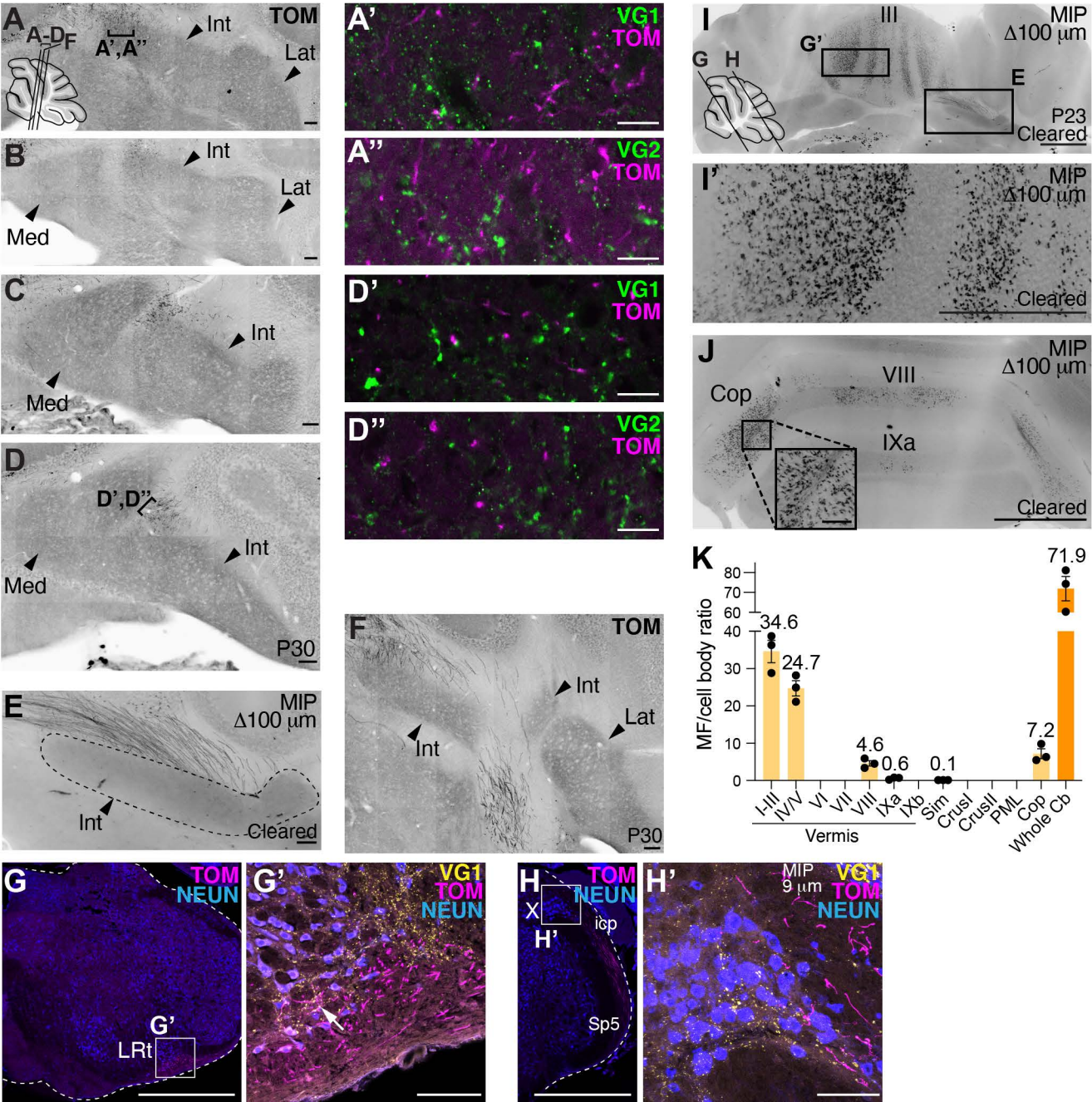
A
A-D
F
A',A''
Int
TOM
Lat
B
Int
Lat
Med
C
Int
Med
D
D',D''
Int
Med
P30
E
MIP
Δ100 μm
Int
Cleared
A'
VG1
TOM
A''
VG2
TOM
D'
VG1
TOM
D''
VG2
TOM
F
TOM
Int
Lat
Int
P30
I
III
MIP
Δ100 μm
G'
G
H
E
P23
Cleared
I'
MIP
Δ100 μm
Cleared
J
MIP
Δ100 μm
VIII
Cop
IXa
Cleared
K
MF/cell body ratio
80
70
60
40
30
20
10
0
34.6
24.7
4.6
0.6
0.1
7.2
71.9
I-III
IV/V
VI
VII
VIII
IXa
IXb
Sim
CrusI
CrusII
PML
Cop
Whole Cb
Vermis
G
TOM
NEUN
G'
LRt
G'
VG1
TOM
NEUN
H
TOM
NEUN
X
H'
icp
Sp5
H'
MIP
9 μm
VG1
TOM
NEUN

Fig. 4

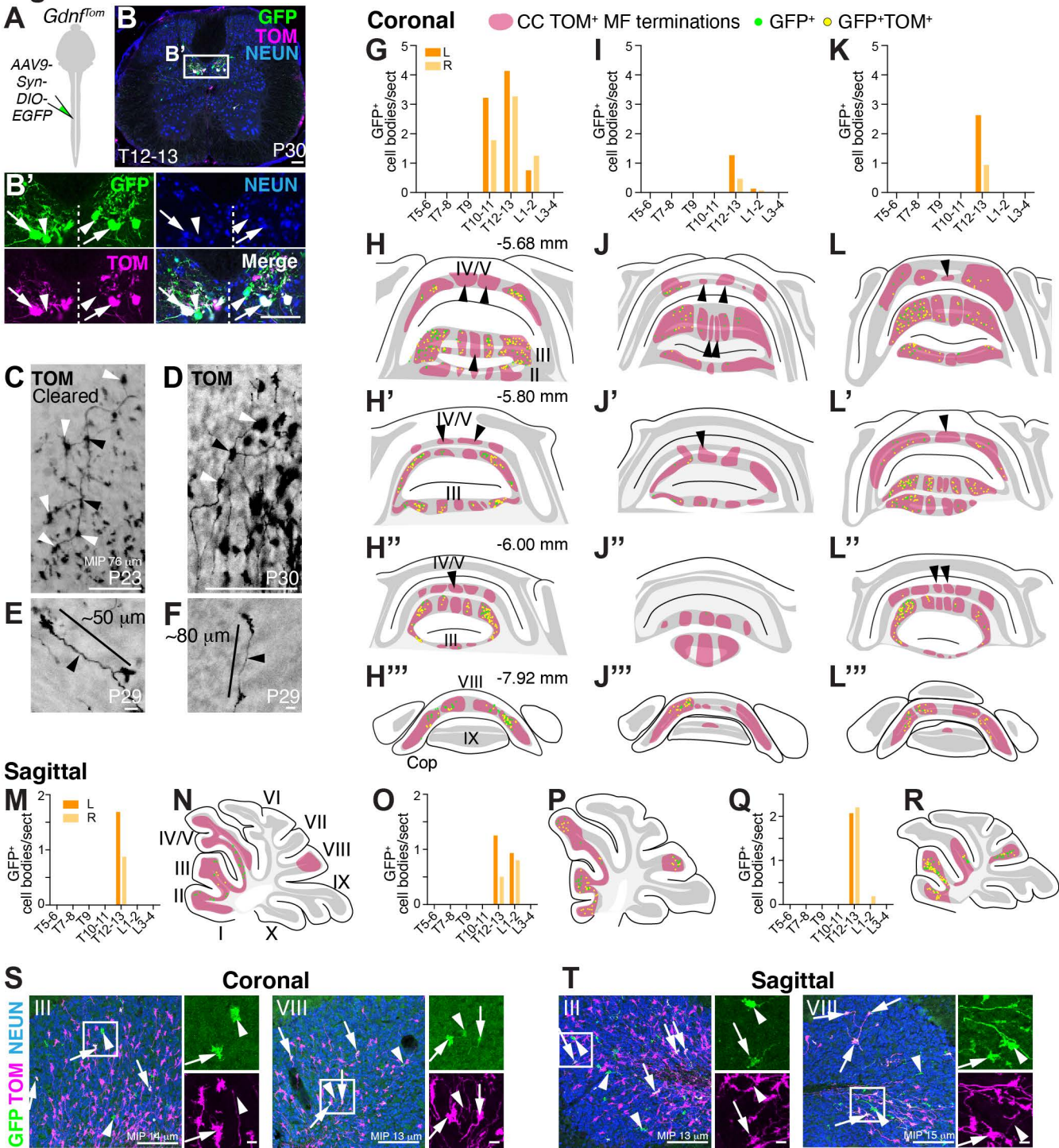
A
Gdnf^Tom
AAV9-Syn-DIO-EGFP
B
GFP
TOM
NEUN
B'
T12-13
P30
B'
GFP
NEUN
TOM
Merge
C
TOM
Cleared
MIP 76 µm
P23
D
TOM
P30
E
~50 µm
P29
F
~80 µm
P29
Coronal
CC TOM+ MF terminations
GFP+
GFP+TOM+
G
I
K
L
R
GFP+ cell bodies/sect
T5-6
T7-8
T9
T10-11
T12-13
L1-2
L3-4
H
-5.68 mm
IV/V
III
II
H'
-5.80 mm
IV/V
III
H''
-6.00 mm
IV/V
III
H'''
-7.92 mm
VIII
IX
Cop
J
J'
J''
J'''
L'
L''
L'''
Sagittal
M
N
VI
VII
VIII
IX
IV/V
III
II
I
X
O
P
Q
R
S
Coronal
III
VIII
MIP 14 µm
MIP 13 µm
GFP TOM NEUN
T
Sagittal
III
VIII
MIP 13 µm
MIP 15 µm

Fig. 5

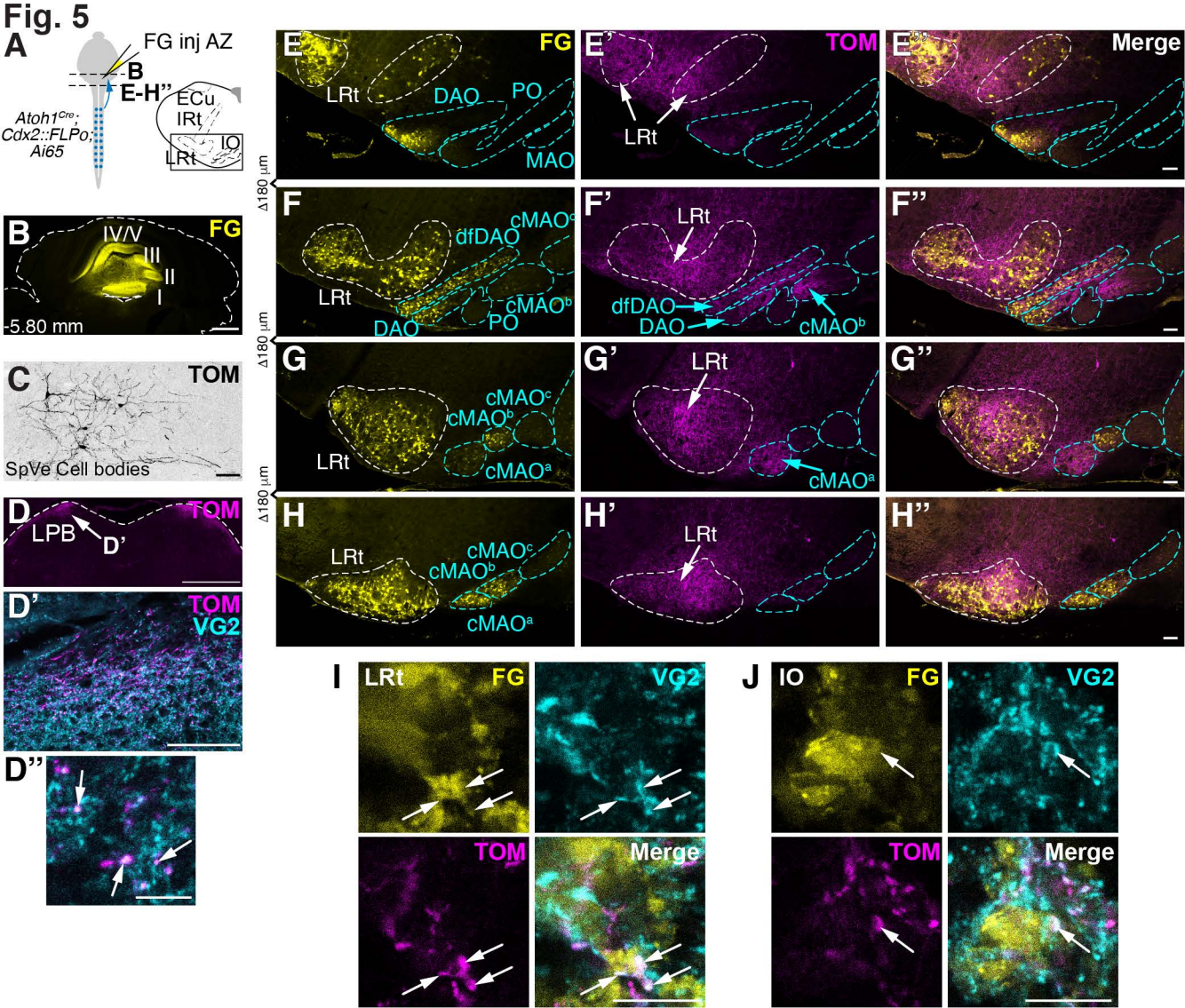
A
FG inj AZ
B
E-H''
ECu
IRt
IO
LRt
Atoh1Cre; Cdx2::FLPo; Ai65
B
FG
IV/V
III
II
I
-5.80 mm
C
TOM
SpVe Cell bodies
D
TOM
LPB
D'
D'
TOM
VG2
D''
E
FG
LRt
DAO
PO
MAO
E'
TOM
LRt
E''
Merge
Δ180 µm
F
dfDAO
cMAOc
LRt
cMAOb
DAO
PO
F'
LRt
dfDAO
DAO
cMAOb
F''
G
cMAOc
cMAOb
LRt
cMAOa
G'
LRt
cMAOa
G''
H
LRt
cMAOc
cMAOb
cMAOa
H'
LRt
H''
I
LRt
FG
VG2
TOM
Merge
J
IO
FG
VG2
TOM
Merge

Fig. 6

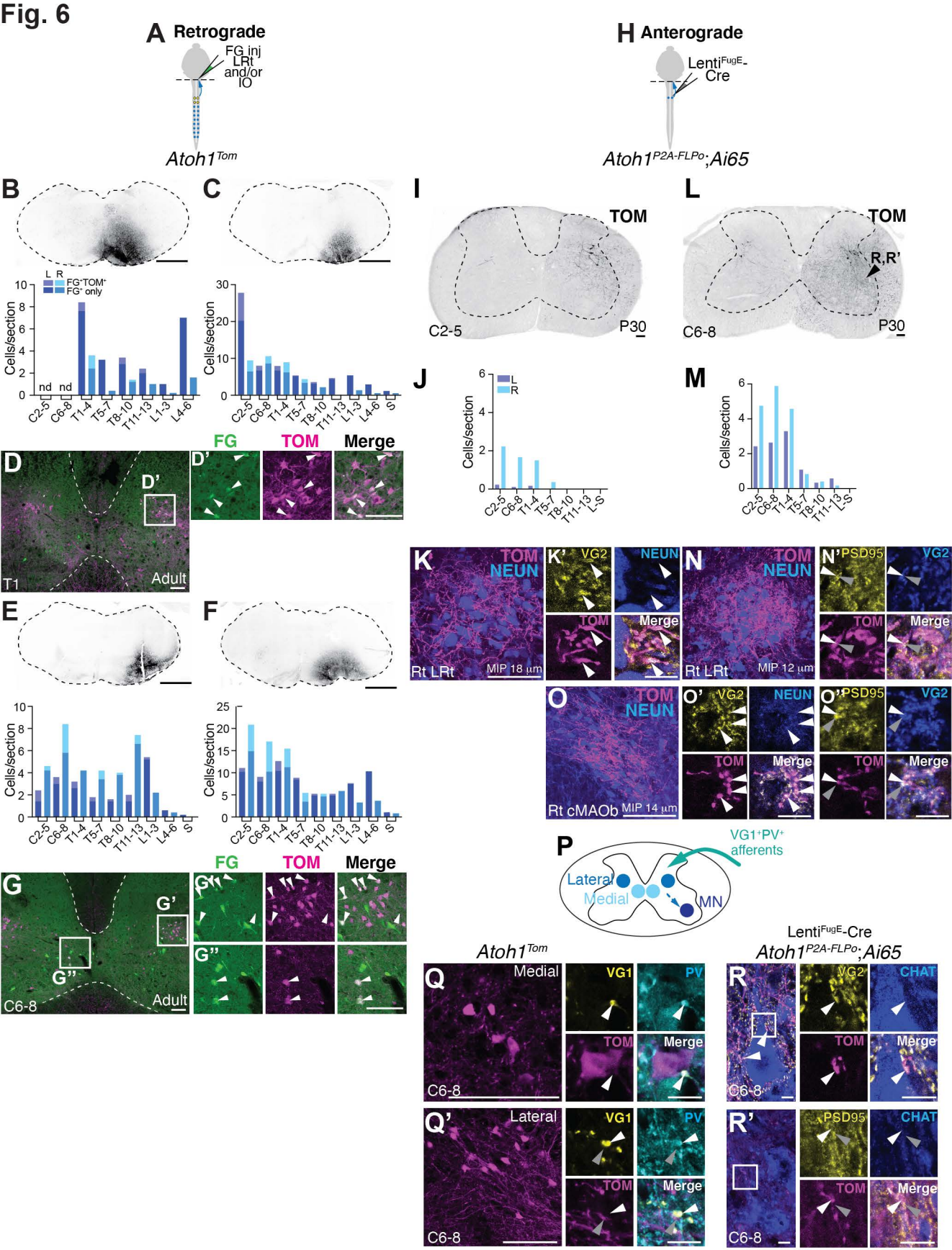
A Retrograde
FG inj
LRt
and/or
IO
Atoh1Tom
H Anterograde
LentiFugE-
Cre
Atoh1P2A-FLPo;Ai65
B
C
L R
FG+TOM+
FG+ only
Cells/section
nd nd
C2-5
C6-8
T1-4
T5-7
T8-10
T11-13
L1-3
L4-6
S
D
D'
FG
TOM
Merge
T1
Adult
E
F
G
G'
G''
C6-8
I
TOM
C2-5
P30
L
R,R'
C6-8
J
M
K
K'
VG2
NEUN
Rt LRt
MIP 18 μm
N
N'
PSD95
MIP 12 μm
O
O'
O''
Rt cMAOb
MIP 14 μm
P
VG1+PV+
afferents
Lateral
Medial
MN
Atoh1Tom
LentiFugE-Cre
Atoh1P2A-FLPo;Ai65
Q
Q'
VG1
PV
R
R'
CHAT

Fig. 7

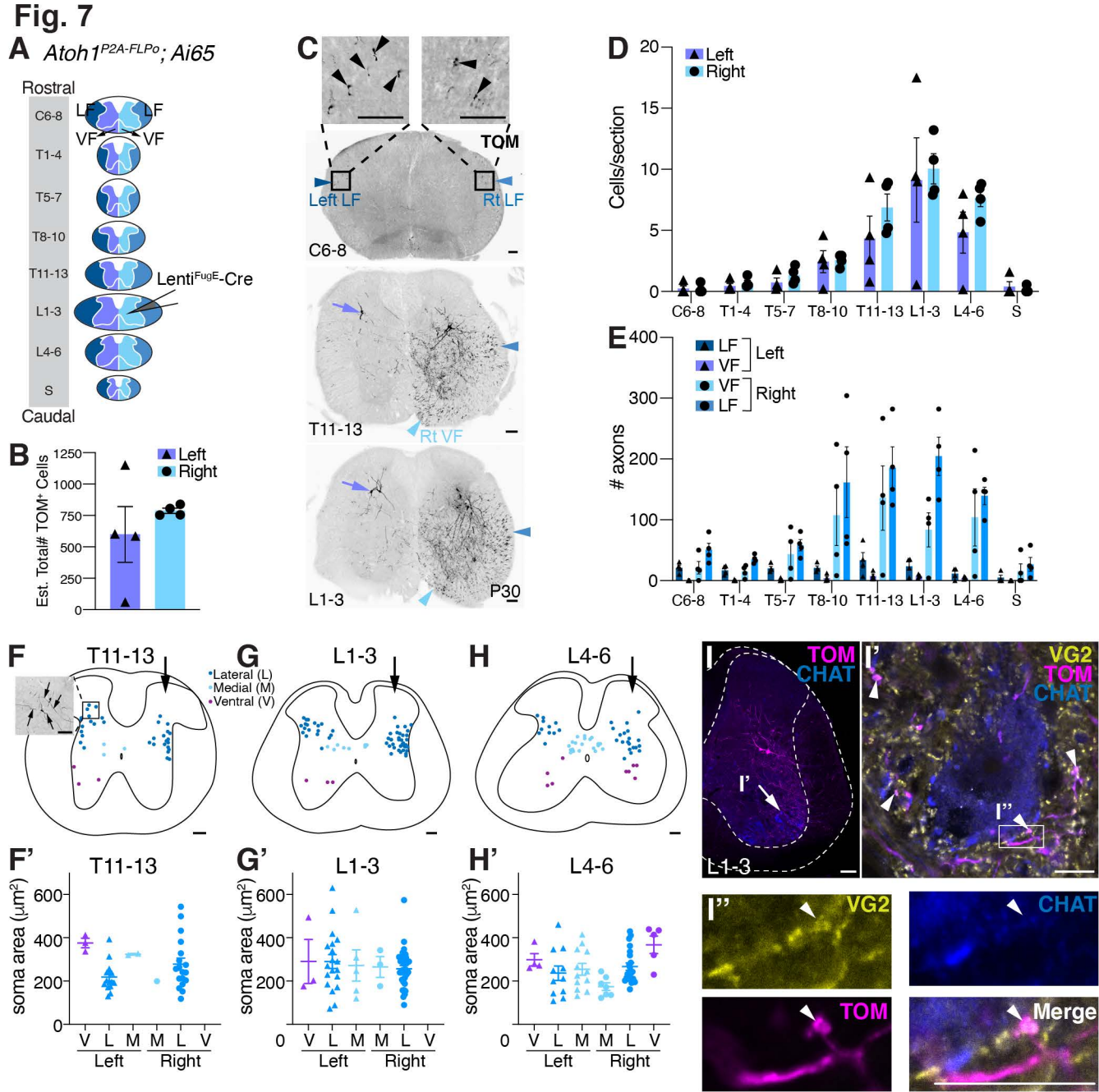
A
Atoh1P2A-FLPo; Ai65
Rostral
C6-8
T1-4
T5-7
T8-10
T11-13
L1-3
L4-6
S
Caudal
LF
VF
LentiFugE-Cre
B
Est. Total# TOM+ Cells
Left
Right
C
TOM
Left LF
Rt LF
C6-8
T11-13
Rt VF
L1-3
P30
D
Cells/section
Left
Right
E
axons
LF
VF
Left
Right
F
T11-13
G
L1-3
H
L4-6
Lateral (L)
Medial (M)
Ventral (V)
F'
G'
H'
soma area (μm2)
V L M M L V
Left
Right
I
TOM
CHAT
I'
L1-3
I''
VG2
TOM
CHAT
Merge

Fig. 8

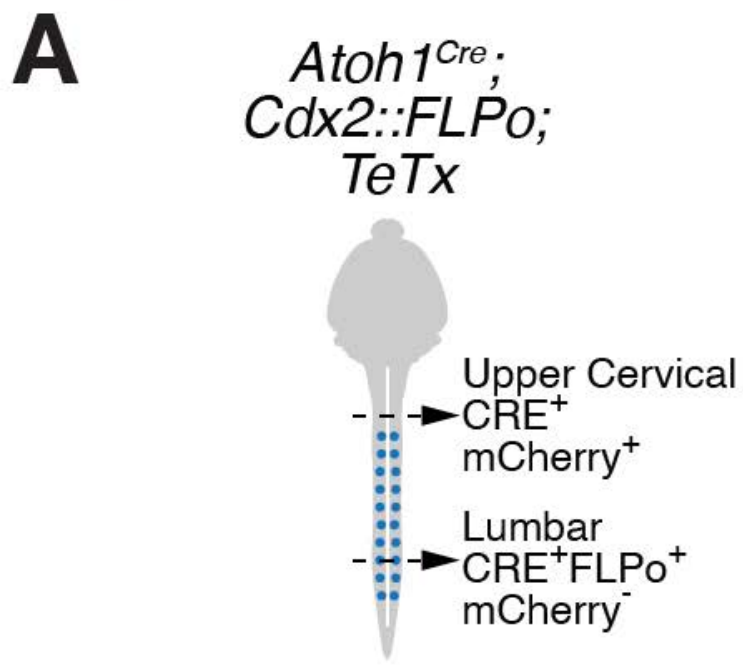
A
Atoh1Cre;
Cdx2::FLPo;
TeTx
Upper Cervical
CRE+
mCherry+
Lumbar
CRE+FLPo+
mCherry-

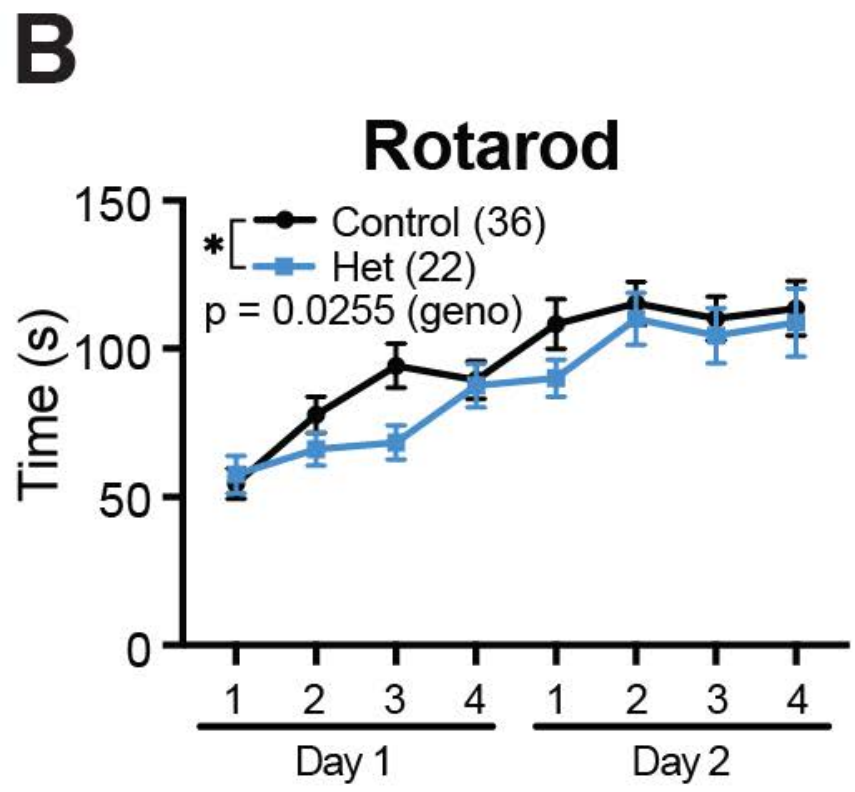
B
Rotarod
Control (36)
Het (22)
p = 0.0255 (geno)
*
Time (s)
150
100
50
0
1
2
3
4
1
2
3
4
Day 1
Day 2

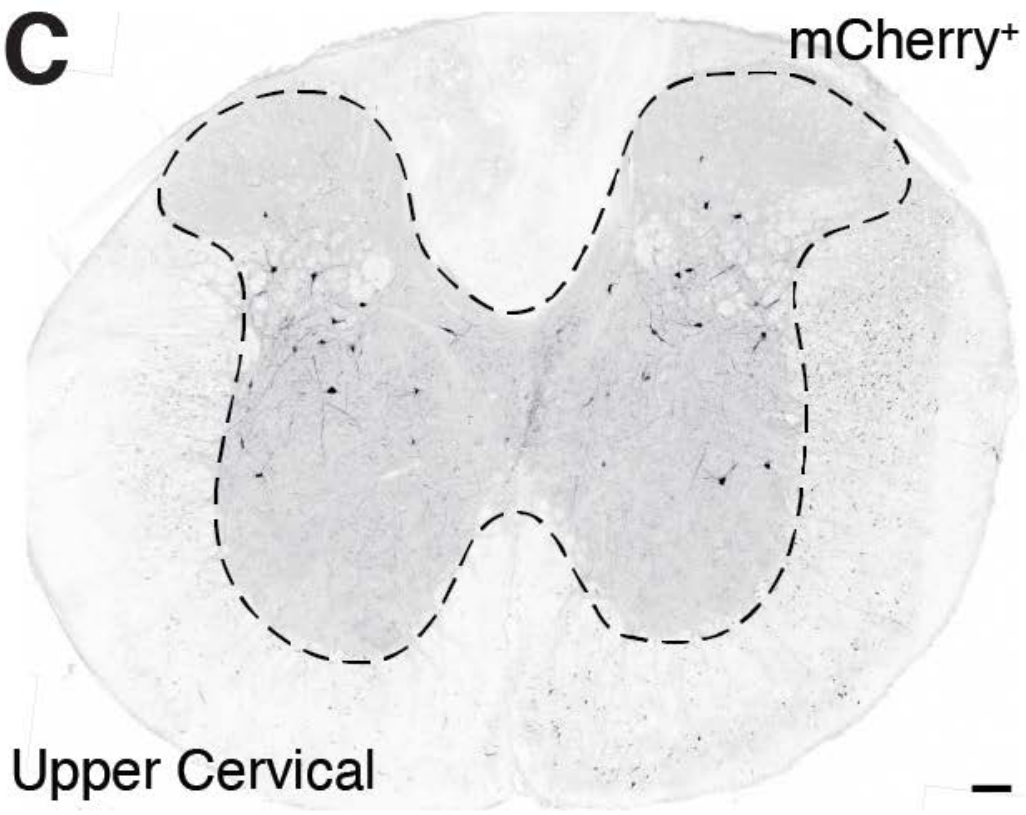
C
mCherry+
Upper Cervical

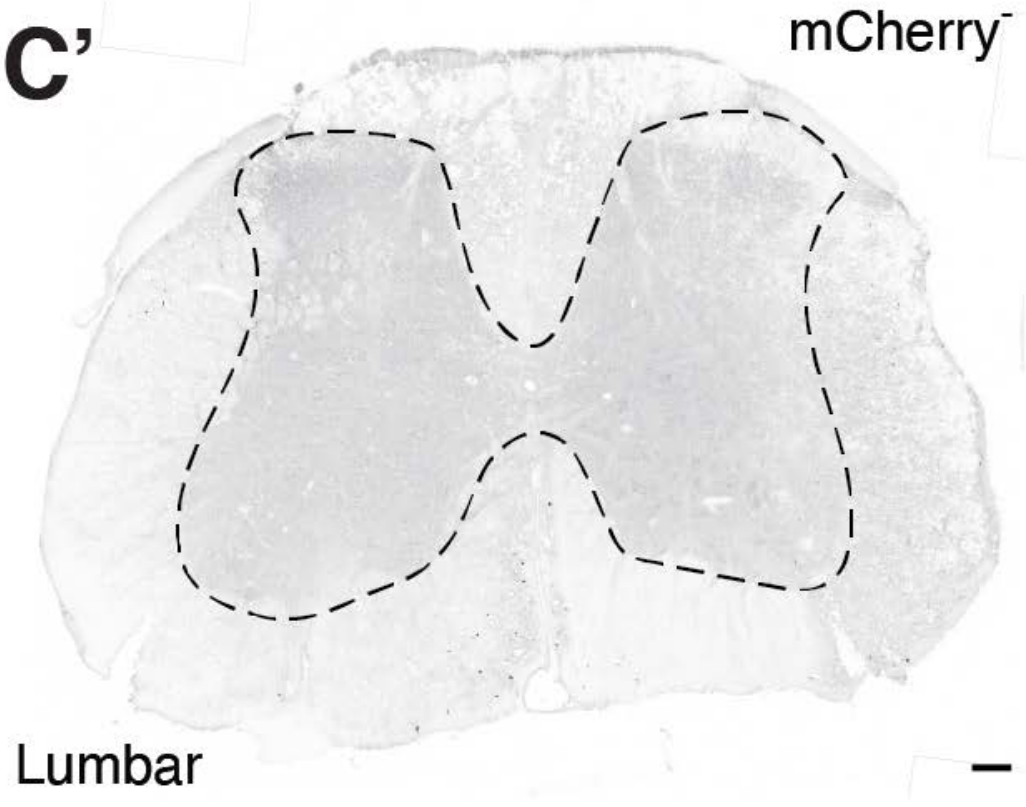
C'
mCherry-
Lumbar

Fig. 9

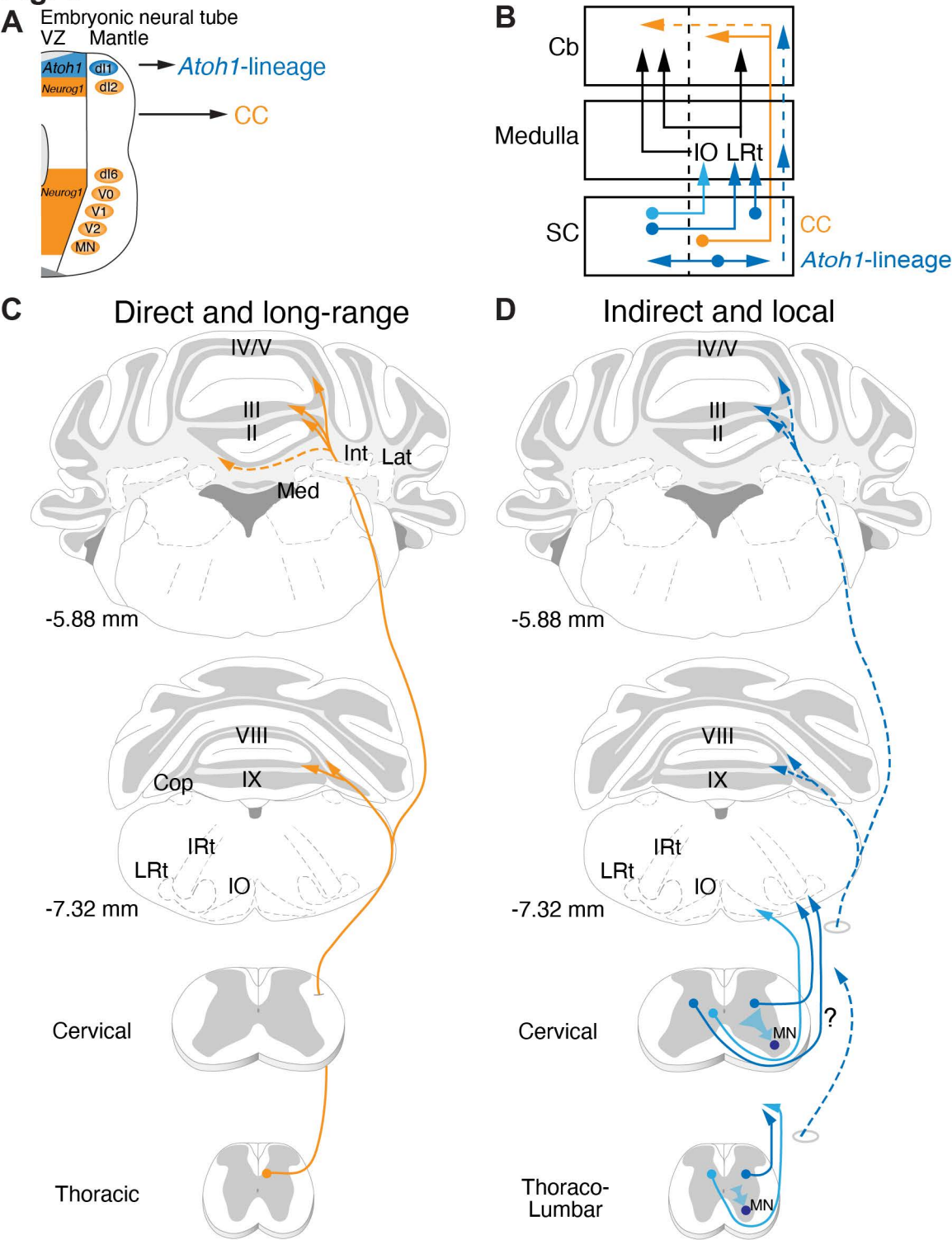
A
Embryonic neural tube
VZ
Mantle
Atoh1
Neurog1
dI1
dI2
Atoh1-lineage
CC
Neurog1
dI6
V0
V1
V2
MN
B
Cb
Medulla
IO
LRt
SC
CC
Atoh1-lineage
C
Direct and long-range
IV/V
III
II
Int
Lat
Med
-5.88 mm
VIII
Cop
IX
IRt
LRt
IO
-7.32 mm
Cervical
Thoracic
D
Indirect and local
IV/V
III
II
-5.88 mm
VIII
IX
IRt
LRt
IO
-7.32 mm
Cervical
MN
?
Thoraco-
Lumbar
MN